



Ricerca di Sistema elettrico

Accoppiamento di codici CFD e codici di sistema in sistemi a piscina ed a loop

G. Barone, N. Forgione, D. Martelli, W. Ambrosini



ACCOPPIAMENTO DI CODICI CFD E CODICI DI SISTEMA IN SISTEMI A PISCINA ED A LOOP

G. Barone, N. Forgione, D. Martelli, W. Ambrosini (UNIFI)

Settembre 2013

Report Ricerca di Sistema Elettrico

Accordo di Programma Ministero dello Sviluppo Economico - ENEA

Piano Annuale di Realizzazione 2012

Area: Produzione di energia elettrica e protezione dell'ambiente

Progetto: Sviluppo competenze scientifiche nel campo della sicurezza nucleare e collaborazione ai programmi internazionali per il nucleare di IV Generazione

Obiettivo: Sviluppo competenze scientifiche nel campo della sicurezza nucleare

Responsabile del Progetto: Mariano Tarantino, ENEA

Il presente documento descrive le attività di ricerca svolte all'interno dell'Accordo di collaborazione "Sviluppo competenze scientifiche nel campo della sicurezza nucleare e collaborazione ai programmi internazionali per il nucleare di IV generazione"

Responsabile scientifico ENEA: Mariano Tarantino

Responsabile scientifico CIRTEN: Giuseppe Forasassi

Titolo

Accoppiamento di codici CFD e codici di sistema in sistemi a piscina ed a loop

PAGINA DI GUARDIA

Descrittori
Tipologia del documento: Rapporto Tecnico

Collocazione contrattuale: Accordo di programma ENEA-MSE su sicurezza nucleare e reattori di IV generazione

Argomenti trattati:

- Termoidraulica dei reattori nucleari
- Termoidraulica del nocciolo
- Analisi di sicurezza
- Generation IV reactors

Sommario

This report, carried out at the DIC (Dipartimento di Ingegneria Civile e Industriale) of Pisa University in collaboration with ENEA Brasimone Research Centre, deals with the modification of the relationship used by the RELAP5 system code to generate the table of LBE, Lead and Sodium and with post-test thermo-fluiddynamic analyses of NACIE loop type (Natural Circulation Experiment) facility and of CIRCEDHR (Circulation Eutectic- Decay Heat Removal System) pool type facility, built at ENEA. Experimental results are compared with those obtained from RELAP5 stand alone calculations and from RELAP5-FLUENT coupled code calculations. In particular, in the first part of this work the equations were modified into RELAP5/Mod3.3 system code to obtain the thermodynamic properties of lead, LBE and sodium and are presented for both saturation and single phase conditions. The second part of this work deals with post-test analyses of the NACIE loop type facility: computational results are obtained both from RELAP5 stand alone and from an in-house coupling tool achieved using RELAP5 thermal-hydraulic system code and CFD Fluent commercial CFD code. After that, a post-test simulation reproducing an accidental event with a total loss of the secondary circuit followed by a reactor scram and DHR system activation to remove residual heat generation, was performed using the RELAP5 code on Test IV of CIRCE facility experiments. Comparative analyses among the simulations performed by RELAP5-Fluent coupled codes and by RELAP5 stand-alone code agreed well, moreover results obtained for the CIRCE-DHR demonstrate the RELAP5 model's suitability in simulating a PLOH+LOF transient representative experiment.

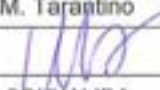
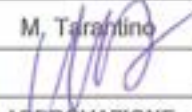
Note

Rapporto emesso da Università di Pisa (UNIPi)

Autori:

G. Barone, N. Forgione, D. Martelli, W. Ambrosini (UNIPi)

Copia n.
In carico a:

0	EMISSIONE	25/09/13	NOME	M. Tarantino	NA	M. Tarantino
			FIRMA			
REV.	DESCRIZIONE	DATA		CONVALIDA	VISTO	APPROVAZIONE



CIRTEN

Consorzio Interuniversitario per la Ricerca TEcnologica Nucleare

UNIVERSITA' DI PISA

DICI

System codes and a CFD codes applied to loop- and pool-type experimental facilities

(Accoppiamento di codici *CFD* e codici di sistema in sistemi a piscina ed a loop)

G. Barone, N. Forgione, D. Martelli, W. Ambrosini

CERSE-UNIFI RL 1530/2013

PISA, September 2013

Lavoro svolto in esecuzione dell'Attività LP2.C1_e
AdP MSE-ENEA sulla Ricerca di Sistema Elettrico - Piano Annuale di Realizzazione 2012
Progetto B.3.1 "Sviluppo competenze scientifiche nel campo della sicurezza nucleare e collaborazione ai programmi internazionali per il nucleare di IV generazione.

Summary

This report, carried out at the *DICI* (Dipartimento di Ingegneria Civile e Industriale) of Pisa University in collaboration with *ENEA* Brasimone Research Centre, deals with the modification of the relationship used by the RELAP5 system code to generate the table of *LBE*, Lead and Sodium and with post-test thermo-fluiddynamic analyses of *NACIE* loop type (Natural Circulation Experiment) facility and of *CIRCE-DHR* (Circulation Eutectic- Decay Heat Removal System) pool type facility, built at ENEA. Experimental results are compared with those obtained from RELAP5 stand alone calculations and from RELAP5-FLUENT coupled code calculations.

In particular, in the first part of this work the equations were modified into RELAP5/Mod3.3 system code to obtain the thermodynamic properties of lead, *LBE* and sodium and are presented for both saturation and single phase conditions.

The second part of this work deals with post-test analyses of the *NACIE* loop type facility: computational results are obtained both from RELAP5 stand alone and from an in-house coupling tool achieved using RELAP5 thermal-hydraulic system code and *CFD* Fluent commercial *CFD* code.

After that, a post-test simulation reproducing an accidental event with a total loss of the secondary circuit followed by a reactor scram and *DHR* system activation to remove residual heat generation, was performed using the RELAP5 code on Test IV of *CIRCE* facility experiments.

Comparative analyses among the simulations performed by RELAP5-Fluent coupled codes and by RELAP5 stand-alone code agreed well, moreover results obtained for the *CIRCE-DHR* demonstrate the RELAP5 model's suitability in simulating a *PLOH+LOF* transient representative experiment.

Index

Summary2
1. Thermodynamic properties used to generate RELAP5 tables for	
<i>LBE</i>, lead and sodium	5
1.1 Liquid phase	5
1.1.1 Saturated vapor pressure.....	5
1.1.2 Saturated vapor temperature	5
1.1.3 Specific volume at atmospheric pressure	5
1.1.4 Specific heat at atmospheric pressure	6
1.1.5 Derivative obtained using approximate correlation only function of temperature	6
1.1.6 Specific volume as a function of temperature and pressure	6
1.1.7 Isobaric coefficient of thermal expansion.....	7
1.1.8 Isothermal coefficient of compressibility.....	7
1.1.9 Specific enthalpy	7
1.1.10 Specific entropy	8
1.2 Vapour phase.....	9
1.2.1 Specific volume	9
1.2.2 Isobaric coefficient of thermal expansion.....	9
1.2.3 Isothermal coefficient of compressibility.....	9
1.2.4 Specific heat at constant volume	9
1.2.5 Specific heat at constant pressure	9
1.2.6 Specific internal energy.....	9
1.2.7 Specific entropy	10
2. Correlations for <i>LMs</i> implemented inside the RELAP5 code	11
2.1 Transport properties	11
2.2 Convective heat transfer correlations	11
3. Description of the <i>NACIE</i> loop facility	13
4. <i>NACIE</i> experimental campaign.....	17
5 Thermal-hydraulic post-test analysis of <i>NACIE</i>	18

5.1 RELAP5 Model	18
5.2 RELAP5 Post-Test Simulations.....	19
6 RELAP5-Fluent coupled calculations	27
6.1 RELAP5 and Fluent models	27
6.2 Coupling procedure.....	30
6.3 Matrix of simulations	31
6.4 Obtained results: Test 206 and Test 306.....	32
7 Thermal-hydraulic post-test analysis of <i>ICE-DHR</i>.....	38
7.1 Post-Test RELAP5 simulations.....	38
7.2 Test IV. Initial and Boundary Conditions	40
7.3 Test IV. <i>PLOH+LOF</i> Simulation Analysis	41
8. Conclusions	46
References	47
Nomenclature	48
 Breve CV del gruppo di lavoro	 50

1. Thermodynamic properties used to generate RELAP5 tables for LBE, lead and sodium

In this section the equations needed to obtain temperature, pressure, specific volume, specific internal energy, thermal expansion coefficient, isothermal compressibility, specific heat at constant pressure and specific entropy are presented for both saturation and single phase conditions. The thermodynamic properties of lead, LBE and sodium have been found in V. Sobolev's work [1]. Properties and coefficients used inside the correlations, where not specified, are reported in SI base units.

1.1 Liquid phase

1.1.1 Saturated vapor pressure

Sobolev [1] reports the following correlation for the saturation pressure as a function of temperature.

$$p_{sat}(T) = a_1 \cdot \exp\left(\frac{a_2}{T}\right) \quad (1.1)$$

where for LBE is $a_1=1.22\text{E}10$ and $a_2= -22552$ and for lead $a_1=5.76\text{E}9$ and $a_2= -22131$. For sodium, the saturation pressure was reported in a more complicated form by Sobolev, but starting from it and using a better fitting method a correlation with the same form used for LBE and lead is derived. In particular, for sodium the two previous coefficients are found to be: $a_1=4.18965\text{E}9$ and $a_2= -1.22805\text{E}4$.

1.1.2 Saturated vapour temperature

As a consequence of the previous correlations, temperature can be written as a function of pressure through the following equation:

$$T_{sat}(p) = \frac{a_2}{\ln\left(\frac{p}{a_1}\right)} \quad (1.2)$$

1.1.3 Specific volume at atmospheric pressure

From Sobolev's work density at atmospheric pressure ($p_{ref} \cong 10^5$ Pa) is given as the following linear function of temperature:

$$\rho_{l,ref}(T) = r_0 + r_1 T \quad (1.3)$$

In the present work the use of polynomial form for the specific volume correlation is preferred. Then, using a least-squares regression method, the Sobolev correlation for density was transformed in the following form:

$$v_{l,ref}(T) = b_0 + b_1 T + b_2 T^2 + b_3 T^3 \quad (1.4)$$

where

$b_0=9.02805304\text{E}-05$, $b_1=1.09001277\text{E}-08$, $b_2=8.44153423\text{E}-13$, $b_3=3.10620231\text{E}-16$ for LBE;
 $b_0=8.73593582\text{E}-05$, $b_1=9.93870088\text{E}-09$, $b_2=8.88207610\text{E}-13$, $b_3=2.24367865\text{E}-16$ for lead;
 $b_0=9.80671847\text{E}-04$, $b_1=2.54530643\text{E}-07$, $b_2=1.23725177\text{E}-11$, $b_3=3.59886201\text{E}-14$ for sodium.

1.1.4 Specific heat at atmospheric pressure

The correlation for the specific heat at atmospheric pressure ($p_{ref} \cong 10^5$ Pa) is given by Sobolev, as a function of temperature, in the form:

$$c_{pl,ref}(T) = e_0 + e_1 T + e_2 T^2 + e_3 T^{-2} \quad (1.5)$$

In the present work the use of a third order polynomial of temperature is preferred. Then, using a regression method, the Sobolev correlation was here transformed in the following form:

$$c_{pl,ref}(T) = d_0 + d_1 T + d_2 T^2 + d_3 T^3 \quad (1.6)$$

where

$d_0=1.57972755E+02$, $d_1=-2.47822044E-02$, $d_2=1.72861218E-06$, $d_3=2.60782635E-09$ for LBE;
 $d_0=1.61791750E+02$, $d_1=-2.31399817E-02$, $d_2=-1.45020777E-06$, $d_3=3.70731445E-09$ for lead;
 $d_0=1.60476754E+03$, $d_1=-7.22160215E-01$, $d_2=3.41613663E-04$, $d_3=2.86782393E-08$ for sodium.

1.1.5 Derivative obtained using approximate correlation only function of temperature

Assuming the enthalpy derivatives only as function of temperature, they can be calculated using the correlation for the specific volume given at reference pressure:

$$\left(\frac{\partial h_l}{\partial p}\right)_T = v_l - T \left(\frac{\partial v_l}{\partial T}\right)_p \cong v_{l,ref} - T \left(\frac{dv_{l,ref}}{dT}\right) = b_0 - b_2 T^2 - 2b_3 T^3 \quad (1.7)$$

$$\left[\frac{\partial}{\partial T} \left(\frac{\partial h_l}{\partial p}\right)_T\right]_p = -T \left(\frac{\partial^2 v_l}{\partial T^2}\right)_p \cong -T \left(\frac{d^2 v_{l,ref}}{dT^2}\right) = -2b_2 T - 6b_3 T^2$$

1.1.6 Specific volume as a function of temperature and pressure

Since the specific volume is a function of temperature and a weak function of pressure the first two terms of the Taylor series can be used to obtain this dependence:

$$\begin{aligned} v_l(T, p) &\cong v_{l,ref}(T) + \left(\frac{\partial v_l}{\partial p}\right)_T (p - p_{ref}) \\ \left(\frac{\partial v_l}{\partial p}\right)_T &\cong -v_{l,ref}(T) \kappa_{l,ref}(T) \\ v_l(T, p) &\cong v_{l,ref}(T) - v_{l,ref}(T) \kappa_{l,ref}(T) (p - p_{ref}) \end{aligned} \quad (1.8)$$

where

$$\kappa_{l,ref}(T) = v_{l,ref} \left(\frac{1}{w_{s,l}^2} + \frac{\beta_{l,ref}^2 T}{c_{pl,ref}} \right) \quad (1.9)$$

with w_s representing the sound velocity obtained from the corresponding correlations given by Sobolev for the three fluids. For each fluid, using the correlations at reference pressure for the specific volume, the isobaric coefficient of thermal expansion and the specific heat, the following third order polynomial for the reference isothermal coefficient of compressibility was derived with a best fit method:

$$\kappa_{l,ref}(T) = v_{l,ref} \left(\frac{1}{w_{s,l}^2} + \frac{\beta_{l,ref}^2 T}{c_{pl,ref}} \right) \quad (1.10)$$

where

$c_0=2.96266725\text{E-}11$, $c_1=7.63414010\text{E-}15$, $c_2=1.33519112\text{E-}17$ for *LBE*;

$c_0=2.48689008\text{E-}11$, $c_1=9.28978837\text{E-}15$, $c_2=1.06789185\text{E-}17$ for lead;

$c_0=1.93389526\text{E-}10$, $c_1=-7.87675461\text{E-}14$, $c_2=2.45166675\text{E-}16$ for sodium.

1.1.7 Isobaric coefficient of thermal expansion

The thermal expansion coefficient was approximated by the following equation:

$$\beta_l(T, p) \cong \frac{1}{v_l(T, p)} \left(\frac{dv_{l,ref}}{dT} \right) = \frac{(b_1 + 2b_2 T + 3b_3 T^2)}{v_l(T, p)} \quad (1.11)$$

1.1.8 Isothermal coefficient of compressibility

The isothermal coefficient of compressibility was evaluated through:

$$\kappa_l(T, p) \cong \frac{v_{l,ref}(T) \kappa_{l,ref}(T)}{v_l(T, p)} = \frac{\kappa_{l,ref}(T)}{1 - \kappa_{l,ref}(T)(p - p_{ref})} \quad (1.12)$$

and then

$$\kappa_l(T, p) = \frac{c_0 + c_1 T + c_2 T^2}{1 - (c_0 + c_1 T + c_2 T^2)(p - p_{ref})} \quad (1.13)$$

1.1.9 Specific enthalpy

The specific enthalpy can be written, in the same way as performed for the specific volume, i.e.:

$$h_l(T, p) \cong h_{l,ref}(T) + \left(\frac{\partial h_l}{\partial p} \right)_T (p - p_{ref}) \quad (1.14)$$

Integrating first between a reference temperature T_{ref} and the generic temperature T for $p=p_{ref}$ and after between p_{ref} and p along $T=\text{const}$ we obtain:

$$h_l(T, p) = h_{l0} + \int_{T_{ref}}^T c_{pl,ref}(T) dT + \int_{p_{ref}}^p \left(\frac{\partial h_l}{\partial p} \right)_T dp \quad (1.15)$$

and then

$$h_l(T, p) = h_{l0} + d_0(T - T_{ref}) + \frac{d_1}{2}(T^2 - T_{ref}^2) + \frac{d_2}{3}(T^3 - T_{ref}^3) + \frac{d_3}{4}(T^4 - T_{ref}^4) + (b_0 - b_2 T^2 - 2b_3 T^3)(p - p_{ref}) \quad (1.16)$$

The latent heat of melting is about 38600 J/kg for *LBE*, 23070 J/kg for lead and 113000 J/kg for sodium, while the specific heat for the solid phase is about 128, 127 and 1234 J/(kg K), respectively. Choosing the value of 273.15 K as reference temperature and assuming the specific enthalpy equal to zero, one can be obtain:

$$h_{l0} = c_{p,solid}(T_{melt} - T_0) + \Delta h_{melt} \quad (1.17)$$

with $T_{ref} = T_{melt}$ and $p_{ref} = 10^5$ Pa.

Now the specific heat at constant pressure can be obtained as:

$$c_{pl}(T, p) \equiv \left(\frac{\partial h_l}{\partial T} \right)_p = c_{pl,ref}(T) + \left[\frac{\partial}{\partial T} \left(\frac{\partial h_l}{\partial p} \right)_T \right]_p (p - p_{ref}) \quad (1.18)$$

with

$$\left[\frac{\partial}{\partial T} \left(\frac{\partial h_l}{\partial p} \right)_T \right]_p = -T \left(\frac{\partial^2 v_l}{\partial T^2} \right)_p \equiv -T \frac{d^2 v_{l,ref}}{dT^2} \quad (1.19)$$

Then

$$c_{pl}(T, p) = c_{pl,ref}(T) - T \frac{d^2 v_{l,ref}}{dT^2} (p - p_{ref}) \quad (1.20)$$

and using the derivative of specific volume one is obtains:

$$c_{pl}(T, p) = d_0 + d_1 T + d_2 T^2 + d_3 T^3 - (2b_2 T + 6b_3 T^2)(p - p_{ref}) \quad (1.21)$$

1.1.10 Specific entropy

The specific entropy can be written as a function of temperature and pressure, similarly to the specific volume and specific enthalpy, as:

$$ds_l = \frac{c_{pl}}{T} dT + \left(\frac{\partial s_l}{\partial p} \right)_T dp \quad (1.22)$$

Knowing that:

$$\left(\frac{\partial s_l}{\partial p} \right)_T = - \left(\frac{\partial v_l}{\partial T} \right)_p \equiv - \frac{dv_{l,ref}}{dT} \quad (1.23)$$

then

$$ds_l = \frac{c_{pl}}{T} dT - \frac{dv_{l,ref}}{dT} dp \quad (1.24)$$

Integrating first between a reference temperature T_{ref} and the generic temperature T for $p=p_{ref}$ and after between p_{ref} and p along $T=const$ we obtain:

$$s_l(T, p) = s_{l0} + \int_{T_{ref}}^T \frac{c_{pl,ref}(T)}{T} dT - \int_{p_{ref}}^p \frac{dv_{l,ref}}{dT} dp \quad (1.25)$$

and then

$$s_l(T, p) = s_{l0} + d_0 \log \left(\frac{T}{T_{ref}} \right) + d_1 (T - T_{ref}) + \frac{d_2}{2} (T^2 - T_{ref}^2) + \frac{d_3}{3} (T^3 - T_{ref}^3) - (b_1 + 2b_2 T + 3b_3 T^2)(p - p_{ref}) \quad (1.26)$$

with

$$s_{l0} = c_{p,solid} \log \left(\frac{T_{melt}}{T_0} \right) + \frac{\Delta h_{melt}}{T_{melt}} \quad (1.27)$$

A reference temperature of 273.15 K, a specific entropy equal to zero, $T_{ref} = T_{melt}$ and $p_{ref} = 10^5$ Pa, were assumed.

1.2 Vapor-phase

In the present work, van der Waals equation of state for the vapour phase of the considered metals, was used.

1.2.1 Specific volume

The equation of state (EOS) is:

$$p = \frac{RT}{v_v - b} - \frac{a}{v_v^2} \quad (1.28)$$

where

$$a = \frac{27 R^2 T_c^2}{64 p_c}, \quad b = \frac{RT_c}{8 p_c}, \quad v_{v,c} = 3b \quad (1.29)$$

and R is equal to 39.935, 40.128 and 361.659 J/(kg K) for *LBE*, lead and sodium, respectively. This *EOS* must be solved iteratively to obtain the specific volume.

1.2.2 Isobaric coefficient of thermal expansion

The thermal expansion coefficient is given by:

$$\beta_v(T, p) = \frac{1}{v_v} \left(\frac{\partial v_v}{\partial T} \right)_p = \frac{v_v - b}{v_v T - \frac{2a}{R} \left(\frac{v_v - b}{v_v} \right)^2} \quad (1.30)$$

1.2.3 Isothermal coefficient of compressibility

The isothermal coefficient of compressibility follows from the equation:

$$\kappa_v(T, p) = -\frac{1}{v_v} \left(\frac{\partial v_v}{\partial p} \right)_T = \frac{-1}{v_v \left[\frac{2a}{v_v^3} - \frac{RT}{(v_v - b)^2} \right]} \quad (1.31)$$

1.2.4 Specific heat at constant volume

Assuming an ideal mono-atomic gas with a constant specific heat at constant volume:

$$c_{vv} = \frac{3}{2} R \quad (1.32)$$

1.2.5 Specific heat at constant pressure

As a consequence of the previous assumption the specific heat at constant pressure can be obtained as:

$$c_{pv}(T, p) = c_{vv} + \frac{T \beta_v^2 v_v}{\kappa_v} \quad (1.33)$$

1.2.6 Specific internal energy

The differential of the function $u = u(T, v)$ is:

$$du_v = \left(\frac{\partial u}{\partial T} \right)_v dT + \left(\frac{\partial u}{\partial v} \right)_T dv \Rightarrow du_v = c_{vv} dT + \left[T \left(\frac{\partial p}{\partial T} \right)_v - p \right] dv \quad (1.34)$$

For the van der Waals EOS is:

$$\left(\frac{\partial p}{\partial T} \right)_v = \frac{R}{v_v - b} \quad \text{and} \quad T \left(\frac{\partial p}{\partial T} \right)_v - p = \frac{2}{v_v^2} \quad (1.35)$$

Integrating first between saturation temperature T_{melt} and the generic temperature T for $v_v = v_{v,sat}$ and after between $v_{v,sat}$ and v_v along $T=const$ it is:

$$u_v(T, p) = u_v(T_{melt}, p_{sat}(T_{melt})) + c_{vv}(T - T_{melt}) + a \left(\frac{1}{v_v(T_{melt}, p_{sat}(T_{melt}))} - \frac{1}{v_v(T, p)} \right) \quad (1.36)$$

In the previous equation the first term in the second member is given by:

$$u_v(T_{melt}, p_{sat}(T_{melt})) = u_l(T_{melt}, p_{sat}(T_{melt})) + h_{fg}(T_{melt}) - p[v_{v,sat}(T_{melt}, p_{sat}(T_{melt})) - v_{l,sat}(T_{melt}, p_{sat}(T_{melt}))] \quad (1.37)$$

with the latent heat of vaporization at T_{melt} equal to 856000, 858600 and 237000 J/kg for LBE, lead and sodium, respectively.

1.2.7 Specific entropy

The same procedure used for the specific internal energy can be used for the specific entropy writing its differential form as:

$$ds_v = \frac{c_{vv}}{T} dT + \left(\frac{\partial p}{\partial T} \right)_v dv \quad (1.38)$$

Integrating first between saturation temperature T_{melt} and the generic temperature T for $v_v = v_{v,sat}$ and after between $v_{v,sat}$ and v_v along $T=const$, it is:

$$\left[s_v(T, p) = s_l(T_{melt}, p_{sat}(T_{melt})) + \frac{h_{fg}(T_{melt})}{T_{melt}} + c_{vv} \log \left(\frac{T}{T_{melt}} \right) + R \log \left(\frac{v_v(T, p) - b}{v_v(T_{melt}, p_{sat}(T_{melt})) - b} \right) \right] \quad (1.39)$$

2. Correlations for *LMs* implemented inside the RELAP5 code

2.1 Transport properties

The transport properties for *LBE*, lead and sodium implemented directly inside the FORTRAN source file of the code are thermal conductivity, dynamic viscosity and surface tension. In particular, in agreement with Sobolev's work [1], the following correlations are used:

- *Thermal conductivity*

$$\begin{aligned} k &= 3.284 + 1.617 \cdot 10^{-2} T - 2.305 \cdot 10^{-6} T^2 && \text{for } LBE \\ k &= 9.2 + 0.011 T && \text{for lead} \\ k &= 104 + 0.047 T && \text{for sodium} \end{aligned} \quad (2.1)$$

- *Dynamic viscosity*

$$\begin{aligned} \mu &= 4.94 \cdot 10^{-4} \exp(754.1/T) && \text{for } LBE \\ \mu &= 4.55 \cdot 10^{-4} \exp(1069/T) && \text{for lead} \\ \mu &= \exp(556.835/T - 0.3958 \ln(T) - 6.4406) && \text{for sodium} \end{aligned} \quad (2.2)$$

- *Surface tension*

$$\begin{aligned} \sigma &= (448.5 - 0.08 T) \cdot 10^{-3} && \text{for } LBE \\ \sigma &= (525.9 - 0.113 T) \cdot 10^{-3} && \text{for lead} \\ \sigma &= (231 - 0.0966 T) \cdot 10^{-3} && \text{for sodium} \end{aligned} \quad (2.3)$$

2.2 Convective heat transfer correlations

Specific convective heat transfer correlations for *LMs* have been implemented inside the RELAP5 code. In particular, in the current modified version of RELAP5/Mod3.3 is the possibility of choosing among the following four different correlations:

- *Seban and Shimazaki (1951) [2]*

$$Nu = 5 + 0.025 Pe^{0.8} \quad (2.4)$$

valid in fully developed turbulent flow inside a pipe and for uniform wall temperature.

- *Cheng and Tak (2006) [3]*

$$Nu = A + 0.018 Pe^{0.8} \quad \text{with} \quad A = \begin{cases} 4.5 & \text{if } Pe < 1000 \\ 5.4 - 9 \cdot 10^{-4} Pe & \text{if } 1000 \leq Pe \leq 2000 \\ 3.6 & \text{if } Pe > 2000 \end{cases} \quad (2.5)$$

valid in fully developed turbulent flow inside a pipe and for uniform heat flux.

- *Ushakov correlation (1977) [4]*

$$Nu = 7.55 \frac{P}{D} - 20 \left(\frac{P}{D} \right)^{-13} + 0.041 \left(\frac{P}{D} \right)^{-2} Pe^{(0.56 + 0.19 \frac{P}{D})} \quad (2.6)$$

valid for fuel pin placed on triangular lattice without spacer grids, for Peclet number in the range of 1-4000 and pitch to diameter ratio in the range of 1.2-2.0.

- *Mikityuk correlation (2009) [5]*

$$Nu = 0.047 \left[1 - \exp \left(-3.8 \left(\frac{P}{D} - 1 \right) \right) \right] \left(Pe^{0.77} + 250 \right) \quad (2.7)$$

valid for fuel pin placed on triangular or square lattice without spacer grids, for Peclet number in the range of 30-5000 and pitch to diameter ratio in the range of 1.1-1.95.

When a liquid metal (*LBE* or lead or sodium) is used as working fluid, a convective boundary condition must be set in the data for heat structures, in Word 3 of Cards 1CCCG501 and 1CCCG601, as reported in the following table (see Input Manual of RELAP5).

Table 2.1: Choice of Correlation in Word 3 of Cards 1CCCG501 and 1CCCG601 of RELAP5 code

Word 3 of Cards 1CCCG501 and 1CCCG601	Correlation
1, 100, 101	Seban and Shimazaki
102	Cheng and Tak
110	Ushakov (set <i>P/D</i> on 801/901 card)
111	Mikityuk correlation (set <i>P/D</i> on 801/901 card)

3. Description of the *NACIE* loop facility

Since 1999 the *ENEA* Brasimone research center has been strongly involved in Heavy Liquid Metal (HLM) technology development, acquiring large competences and capabilities in the field of *HLM* thermal-hydraulic, coolant technology, material for high temperature applications, corrosion and material protection, heat transfer and removal, component development and testing, remote maintenance, procedure definition and coolant handling.

In this frame, the Natural Circulation Experiment (*NACIE*) has been set up to qualify and characterize components, system and procedures relevant for *HLM* nuclear technologies. In particular, *NACIE* facility sees several experiments performed in the field of thermal hydraulics and fluid dynamics in order to obtain heat transfer correlation in prototypical fuel bundle simulators. *NACIE* experimental campaign is essential for GEN IV nuclear power plant design and for the qualification and development of *CFD* code and Thermal-Hydraulics system code.

NACIE [6], [7] is a loop type facility filled with Lead-Bismuth Eutectic (*LBE*). It basically consists of a rectangular loop made of two vertical stainless steel (AISI 304) pipes (Nominal Pipe Size (*NPS*) 2½" schedule 40) acting as riser and downcomer connected by means of two horizontal pipes of the same dimension. The heat source is installed in the bottom part of the riser, while the upper part of the downcomer is connected through appropriate flanges to a heat exchanger (see Figure 3.1). The overall height measured between the axis of the upper and lower horizontal pipes is 7.5 m and the width is 1 m. The total inventory of *LBE* is in the order of 1000 kg and the loop is designed to work with temperature and pressure of about 550°C and 10 bar respectively. The facility can work both in natural and forced circulation conditions; furthermore the transition from forced to natural circulation can be investigated. Regarding the operation under natural circulation regime, the thermal centers elevation ($H \approx 5.7$ m) between the heat source (*FPS*) and the heat sink (Heat Exchanger, *HX*) provides the pressure head $\Delta p \sim g\beta\Delta T \cdot H$ required to guarantee a suitable *LBE* mass flow rate.

To promote the *LBE* mass flow rate along the loop under forced circulation condition, a gas lift technique was adopted. A pipe with an *I.D.* of 10 mm is housed inside the riser connected through the top flange of the expansion gas to the argon feeding circuit, while at the lower section of the pipe, a nozzle is installed to inject argon into the riser promoting enhanced circulation inside the loop. The Gas injection system is able to supply argon flow rate in the range 1-75 NI/min with a maximum injection pressure of 5.5 bar. The argon gas flows into the riser and it is finally separated (in the expansion gas) from the double phase mixture, flowing upwards into the cover gas while the *LBE* flows into the heat exchanger through the upper horizontal branch. According to the described configuration, the maximum *LBE* mass flow rate is around 5 kg/s in natural circulation and 20 kg/s in forced circulation condition.

The primary *LBE* side is coupled to the water secondary side by means of “tube in tube” counter flow type heat exchanger (*HX*) fed by water at low pressure (about 1.5 bar). It was designed assuming a thermal duty of 30 kW adopting tube-in-tube technology with *LBE* tube side, water shell side and steel powder filling the gap. The *HX* essentially consists of three coaxial tubes with different thicknesses (see Table 3.1 and Figure 3.2). *LBE* flows downward into the inner pipe of the *HX*, while water flows upwards in the annular region between the middle and the outer pipe allowing a counter current flow heat exchange. The annular region between the inner and middle pipes is filled with stainless steel powder. The aim of this powder gap is to ensure the thermal flux between *LBE* and water and to reduce the thermal stress across the tube walls (the thermal gradient between *LBE* and water is localized across the powder layer). Moreover the three pipes are welded together in the lower section while in the upper section, the inner pipe is mechanically decoupled from the other pipes allowing axial expansion between them.

In order to avoid a powder leakage, the annular region (filled by the powder) is closed in the upper section by a graphite stopper. In the outer pipe an expansion joint is installed to mitigate the stresses due to different axial expansion between the middle and the outer pipe walls.

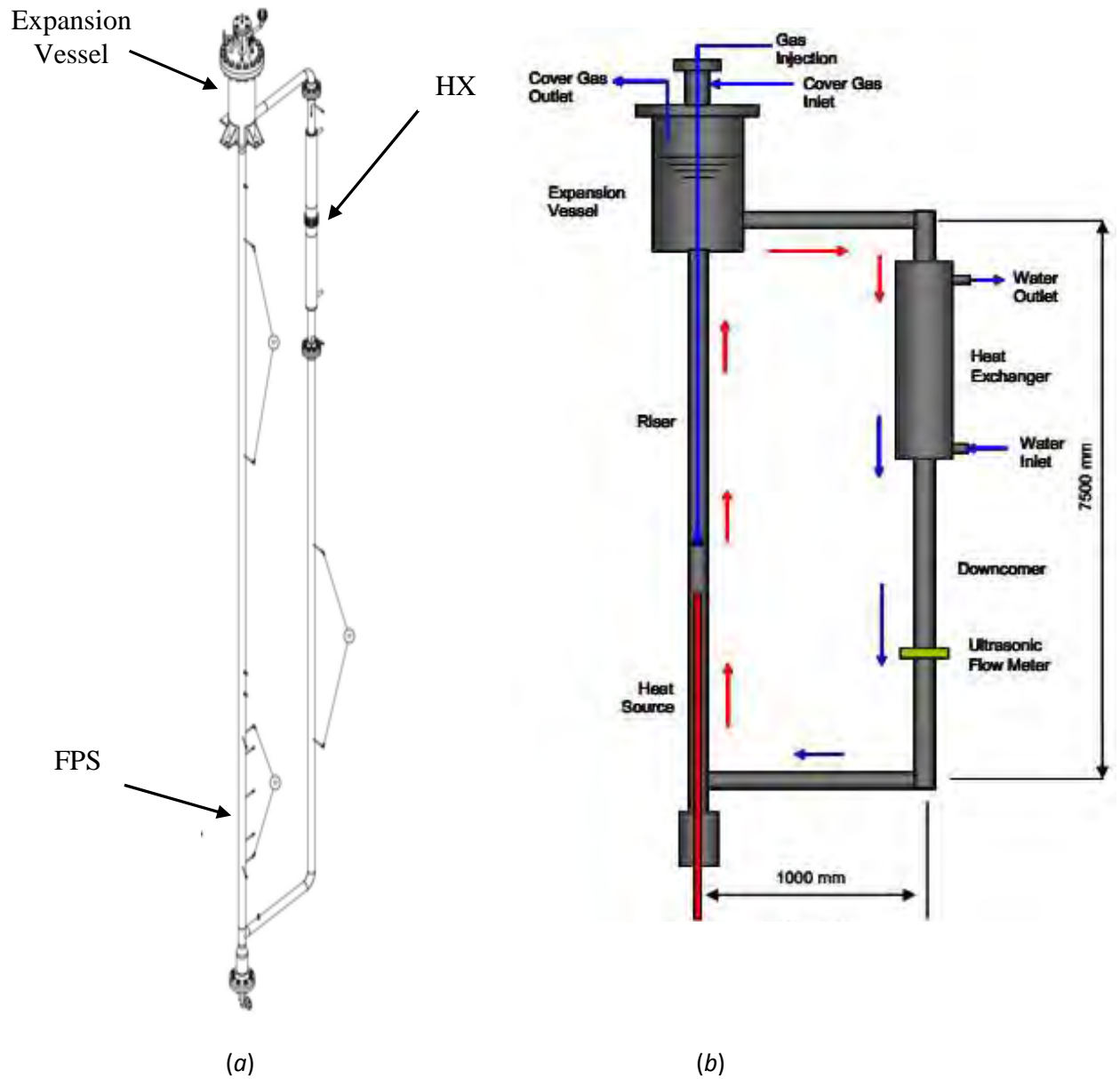


Figure 3.1: Isometric view (a) and layout (b) of the primary loop of the NACIE facility

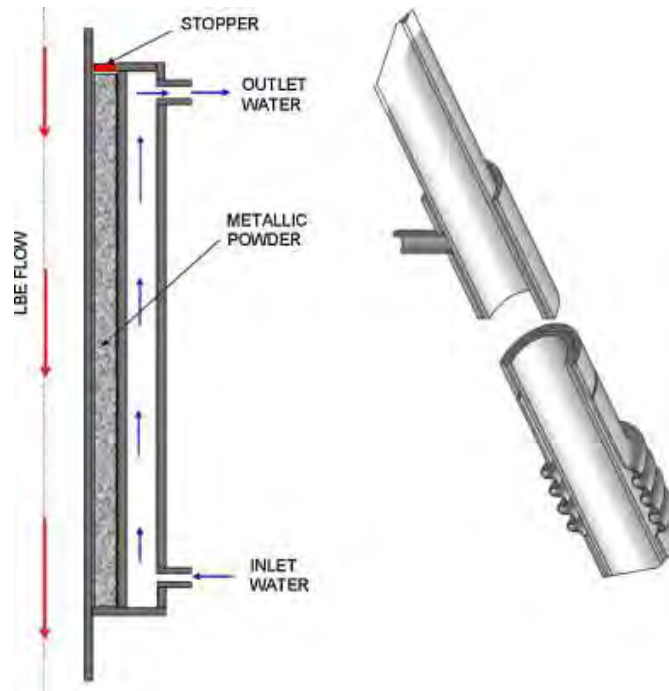


Figure 3.2: NACIE heat exchanger

Table 3.1: NACIE heat exchanger geometrical data

	Inner Pipe	Middle pipe	External pipe
I.D.	62.68 mm	84.9 mm	102.3 mm
O.D.	73 mm	88.9 mm	114.3 mm
Thickness	5.16 mm	2.0 mm	6.02 mm
L	1500 mm	1500 mm	1500 mm
Material	AISI 304	AISI 304	AISI 304

The secondary circuit is then completed by a fan cooler to maintain water temperature under the boiling point (see Figure 3.3).



Figure 3.3: Fan cooler of the secondary circuit

The *NACIE* bundle (see Figure 3.4) consists of two high thermal performance electrical pins with a nominal thermal power of about 43 kW; the main characteristics of the bundle are summarized in Table 3.2.

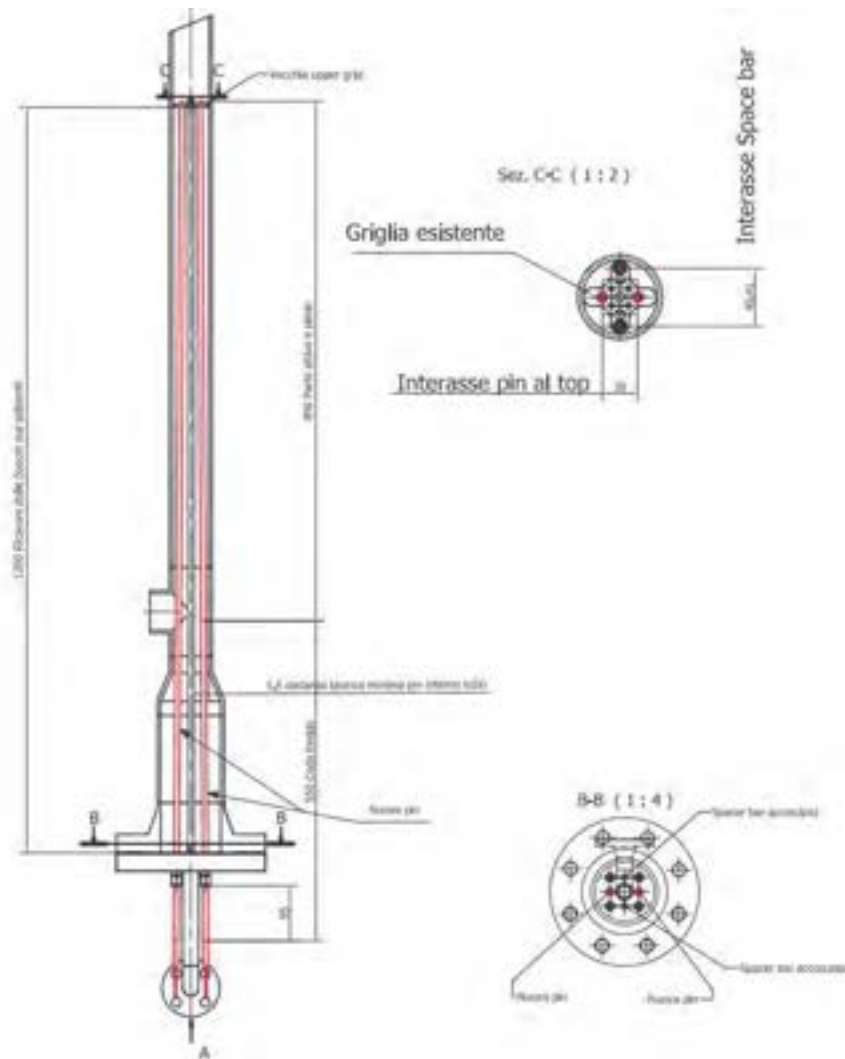


Figure 3.4: *NACIE* electrical fuel pin bundle

Table 3.2: *NACIE* bundle main data

N° of active pins	2
O.D.	8.2 mm
Total length	1400 mm
Active length	850 mm
Heat flux	100 W/cm ²
Thermal Power	22 kW

4. NACIE experimental campaign

The last experimental activity performed on the *NACIE* loop [8] included a series of 10 test concerning natural circulation, forced circulation and transition from forced to natural condition and vice-versa. Each test has been performed with only one pin activated in the heating section, with a maximum nominal power of 21.5 kW. In Table 4.1 the test matrix adopted for the experimental campaign is reported.

Table 4.1: Test matrix

Name	T_{av} [°C]	Power %	Power [kW]	Ramp t [min]	Heat sink	G_lift [NI/min]	Transition NC to FC	Transition FC to NC
201	200-250	50	9.5	5	YES	0	NO	NO
203	200-250	50	9.5	5	YES	5	NO	YES
204	200-250	50	9.5	5	YES	2,4,5,6,8, 10,6,5,4,2	YES	NO
206	200-250	0	0	-	NO	2,4,5,6,8, 10,6,5,4,3	NO	NO
301	300-350	100	21.5	5	YES	0	NO	NO
303	300-350	100	21.5	5	YES	5	NO	YES
304	300-350	100	21.5	5	YES	2,4,5,6,8, 10,6,5,4,2	YES	NO
305	300-350	50	9.5	5	YES	0	NO	NO
306	300-350	0	0	-	NO	2,4,5,6,8, 10,6,5,4,2	NO	NO
406	350-360	25	3.5	5	NO	2,4,5,6,8, 10,6,5,4,2	NO	NO

In Table 4.1, “Name” indicates the case name, T_{av} is the average reference temperature of *LBE* in the loop, “Power” is the power supplied to the Fuel Pin bundle Simulator (*FPS*), Ramp t is the time to reach the bundle power, “Heat Sink” is the activation of the secondary side (Yes= the secondary side and the *HX* are active as heat sink), G_lift is the gas-lift volumetric flow rate and the last two columns refers to the transition from Natural Circulation (*NC*) to Gas Lift Circulation (*FC*) or vice-versa during the specific test.

In the present work test 303 has been used to assess the *NACIE* RELAP5 model, according to the facility experimental setup previously described. The so obtained nodalization has then been used to perform coupled calculations (RELAP5/Fluent) based on the test 206 and test 306.

5 Thermal-hydraulic post-test analysis of *NACIE*

5.1 RELAP5 Model

The *NACIE* loop facility was modelled, on the basis of the configuration previously described, employing RELAP5/Mod3.3 [9] modified to implement *LBE* thermal fluid dynamics properties as reported in Section 2. Figure 5.1 depicts the adopted RELAP5 nodalization scheme: primary *LBE* loop and secondary water cooling circuit can be identified.

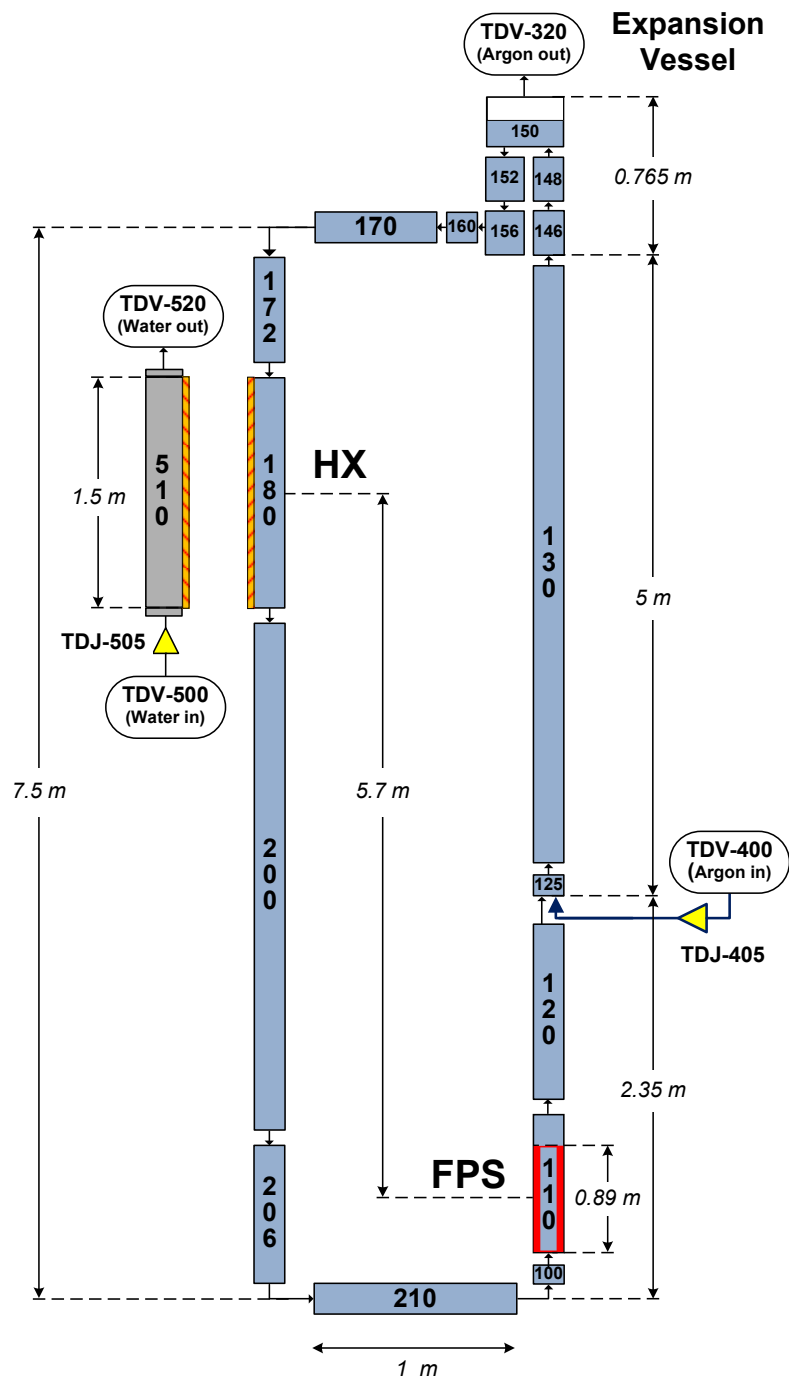


Figure 5.1: RELAP5 Nodalization for the *NACIE* loop

The amount of *LBE* inside the loop is about 835 kg at an initial temperature of 284°C. Argon upper plenum pressure in the Expansion Vessel is set to $1.2 \cdot 10^5$ Pa (*TmdpVol-320*). Referring to the sketch, liquid metal follows an anticlockwise flow path through the loop components. *LBE* receives the supplied power flowing through *Pipe-110* (*FPS*, Fuel Pin Simulator) placed in the bottom section of the Riser; *FPS* active length is characterized by a height of 0.89 m; a single electrical pin supplying heating power is simulated. Gas lift circulation has been modelled using *TmdpJun-405* which connects *TmdpVol-400* (containing argon) to *Branch-125*, injecting the required argon flow into the Riser (2.35 m from the bottom) and thereby promoting *LBE* circulation along the loop. Inside the Expansion Vessel argon is separated from the liquid metal and exits in *TmdpVol-320*; then, from the Expansion Vessel, *LBE* goes through the upper horizontal pipe (*Pipe-160* and *Pipe-170*) to the downcomer where it flows downwards through the Heat Exchanger (*HX*) primary side section (*Pipe-180*, located on the downcomer upper zone). Here power is removed by the secondary side water flowing upwards, thermally coupled to the descending *LBE*. Secondary side water system is modelled by means of *TmdpVol-500*, (where the inlet water properties are set) connected to *TmdpJun-505*, that defines the inlet water mass flow rate feeding the *HX* secondary side annular zone (*Annulus-510*); water flows upwards and exits in *TmdpVol-520*. Primary to secondary heat transfer involves the 1.5 m *HX* active length and simulates the tube in tube counter flow heat exchanger configuration, taking into account the presence of stainless steel powder filling the gap created by the internal and middle pipe (5.95 mm width) described above (see Table 3.1 and Figure 3.2). Thermal conductivity of the powder has been chosen to be 10% of AISI 304 theoretical value. External heat losses have been considered as well. Taking into account the facility thermal insulation, a heat transfer coefficient with external environment, $h^{ext}=1$ W/m²K, has been imposed.

5.2 RELAP5 Post-Test Simulations

The experimental campaign carried out on *NACIE* loop consists of a series of 10 tests aiming at investigating the thermal hydraulic behaviour of the facility under natural circulation, forced circulation and the transition between the two regimes (see Table 4.1). The RELAP5 post-test simulations here analyzed focus on Test 303 designed to reproduce an Unprotected Loss of Flow (*ULOF*) like scenario. Table 5.1 summarizes the sequence of events characterizing the test.

Table 5.1: Test 303

	Time [h]	Action	Description
t_0	0.0	Test starts	<i>LBE</i> loop at rest. Initial temperature = 284°C
t_1	1.28	Argon on	Activation of argon injection. Set flow = 5 NI/min.
t_2	1.78	<i>FPS</i> on	Heat power supplied to fuel pin simulator. Mean power = 21.5 kW
t_3	1.86	<i>HX</i> on	Activation of Heat Exchanger. Secondary water supply = 0.42 m ³ /h
t_4	5.85	Argon off	ULOF event. Argon injection Shut off
t_5	7.60	<i>FPS</i> and <i>HX</i> off	Deactivation of heat power supply to <i>FPS</i> and feedwater to <i>HX</i>

In the following, the time trends of boundary conditions set in RELAP5 input deck are compared with experimental data. Figure 5.2 shows the argon flow injected into the riser of *NACIE* to enhance *LBE* circulation. The experimental trends are measured by a gas flowmeter F101, while the value of 5 NI/min has been adopted in RELAP5 simulation as reference for the gas mass flow rate provided by *TmdpJun-405* for this test.

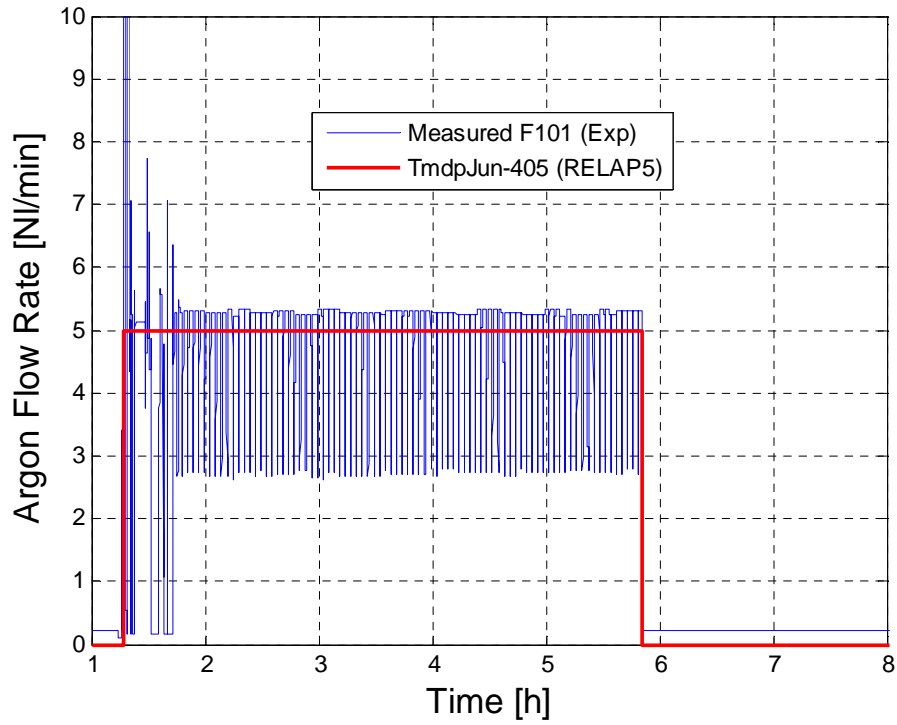


Figure 5.2: Argon flow rate time trend. Comparison of measured and value set by RELAP5

Electric power supplied during Test 303 to the pin simulator is plotted, as a function of time, in Figure 5.3 with heating power set in RELAP5 input deck. Electrical heating starts at $t_2=1.78$ h, increasing linearly to the value of 21 kW in about 2 minutes. Afterwards the power profile shows a non constant trend especially in the first 2 hours from *FPS* activation. Power supply stops at $t_5=7.6$ h.

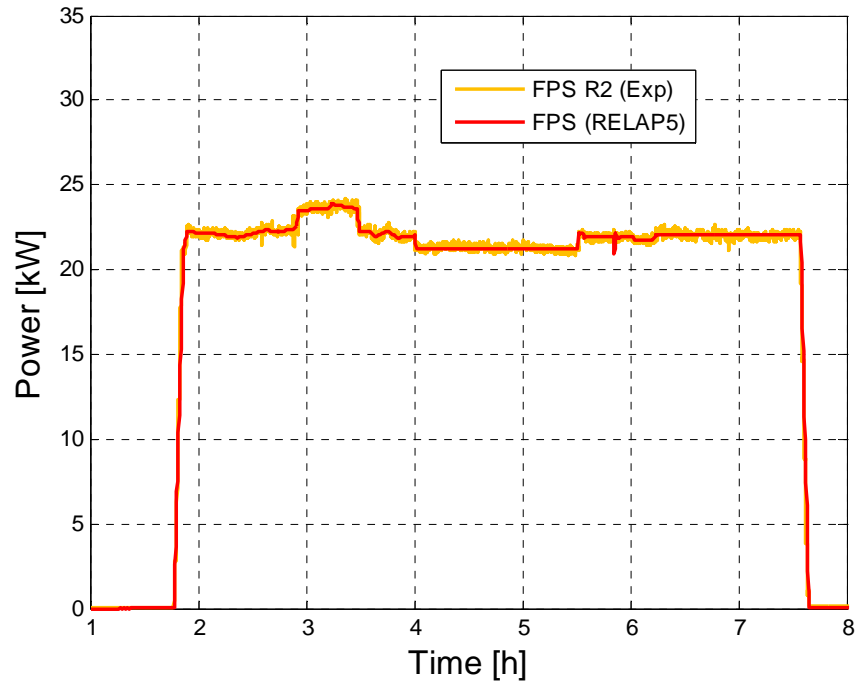


Figure 5.3: Trends of electrical power supplied to FPS and imposed by RELAP5

The *FPS* power time trend in RELAP5 has been reproduced with high accuracy in order to obtain reliable results from the model; indeed, imposing a *FPS* average power (about 21.5 kW) produced considerable discrepancies on temperature profiles (discussed later on). It was assumed that the

measured electric power (R2) was entirely released, through the *FPS*, to the liquid metal. Heat Exchanger water mass flow rate as a function of time (experimentally measured by flowmeter MP201) has been taken to set RELAP5 boundary condition for the secondary water loop, that is, mass flow rate vs time (*TmdpJun-505*). *HX* is activated at $t_3=1.86$ h and operates at $t_5=7.6$ h. The two trends are plotted in Figure 5.4. Heat Exchanger feedwater is injected immediately after *FPS* activation and stops when *FPS* power is shut off. Inlet water mass flow rate is approximately equal to 0.12 kg/s.

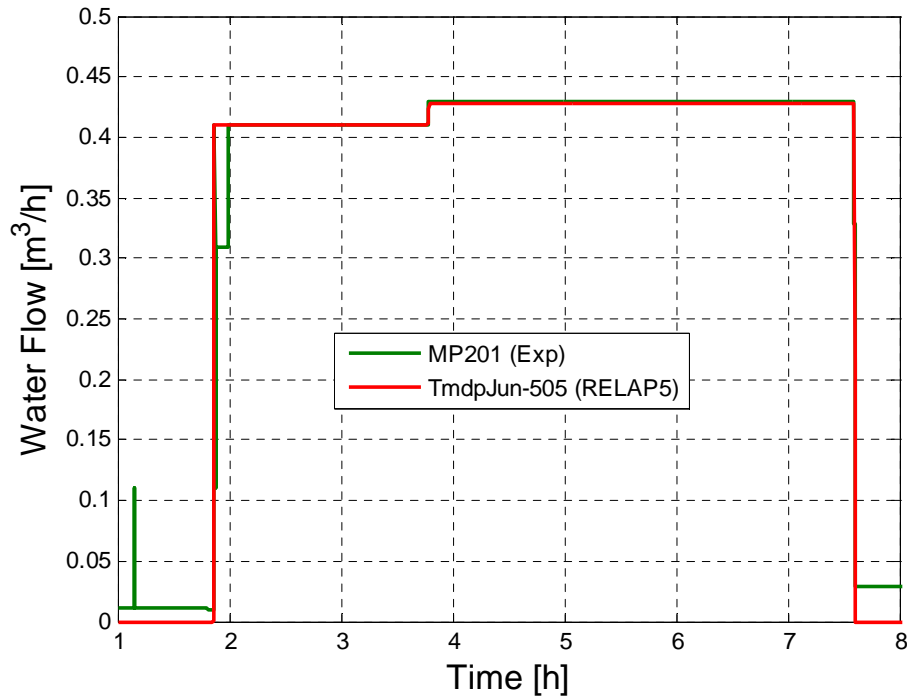


Figure 5.4: Water Flow; comparison of measured and RELAP5 trends

Figure 5.5 depicts *LBE* mass flow rate established during Test 303 in *NACIE* loop, both measured by the inductive flow meter MP101 and indirectly computed using the energy balance across the *FPS*. RELAP5 simulation results are compared to experimental data. *LBE* starts to circulate as argon injection starts (enhanced circulation); afterward, to simulate an *ULOF* accident, argon injection is deactivated ($t_4=5.85$ h) and the flow is then solely driven by buoyancy phenomena (natural circulation). The vertical thermal centres (*FPS* and *HX*) distance is estimated to be 5.7 m. During the enhanced circulation regime, the measured mass flow rate reaches a mean value of about 13 kg/s characterized by oscillating behaviour mainly due to the argon injection compressor system, while heat balance evaluation gives a slightly lower value of about 12 kg/s, very close to the value estimated by the RELAP5 code. Afterward; in natural circulation regime, the mass flow rate drops to about 5 kg/s and good agreement can be observed between experimental data and RELAP5 results. After deactivation of *FPS* and *HX* at t_5 the flow slowly decreases to zero.

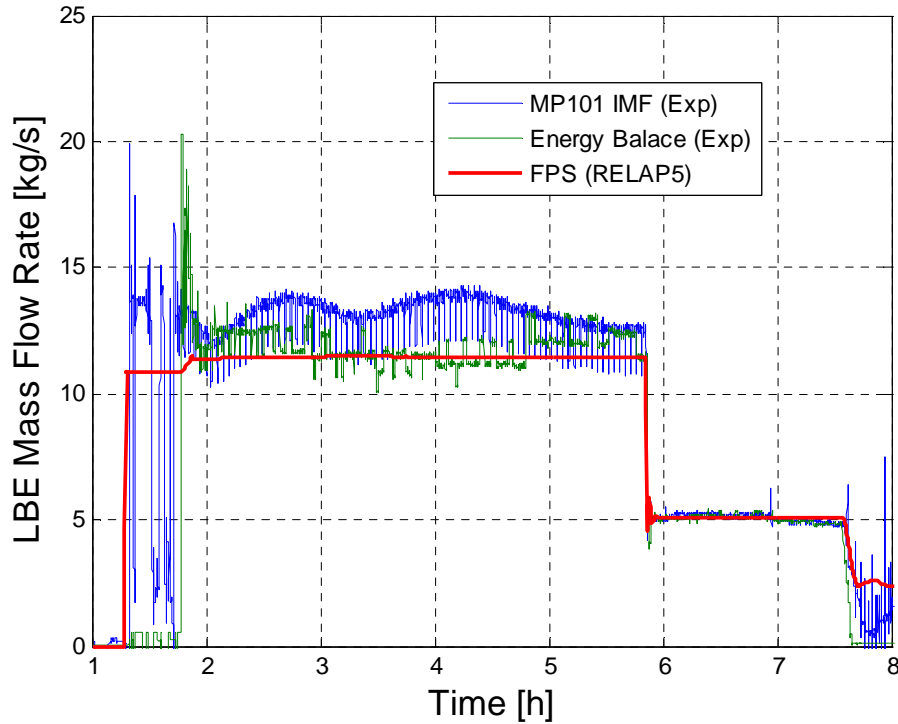


Figure 5.5: LBE mass flow rate: comparison among measured, energy balance and RELAP5 trends

LBE temperature profiles related to FPS inlet and outlet are plotted in Figure 5.6. Experimental values provided by thermocouples T109 (inlet) and T105 (outlet) are compared to RELAP5 results showing good agreement. RELAP5 initial LBE temperature has been set to 284°C for the whole loop assumed adiabatic till the FPS activation, to account for the external wire heaters employed in the experimental setup which maintain the required LBE temperature. Afterwards, a heat transfer coefficient towards the environment has been imposed setting the external air temperature and heat transfer coefficient, respectively equal to 20°C and 1 W/m²K. Following FPS and HX activation, temperatures start to increase up to a mean temperature of about 335°C ($t=3.5$ hours), then temperatures decrease reaching a near stationary condition (mean temperature of 320°C). It can be observed that the temperature profile reflects the power supply variation (see Figure 5.3); accuracy in reproducing FPS experimental power trend in RELAP5 model is mandatory to obtain adequate temperatures profile from the code. At this point ULOF event takes place deactivating gas injection ($t_4=5.85$ h) and natural circulation establishes inside the loop. Inlet/outlet temperatures underwent a sudden decrease/increase of about 10°C followed by an ascending trend up to a new equilibrium value (after less than 2 hours) of 320°C and 348°C respectively, achieving a stationary state for this new regime. FPS and HX are then shut off (at $t_5=7.6$ h) producing a rapid decrease of temperatures due to loop heat losses. RELAP5 outcome adequately reproduces the temperature profile characterizing the test and the transition from forced to natural regimes although slight discrepancies are observed mainly during ULOF transient phase. Experimental and RELAP5 inlet and outlet FPS temperature difference (from previous results) are plotted in Figure 5.7 showing good agreement. Figure 5.8 plots Heat Exchanger measured and simulated secondary water inlet and outlet temperatures. Experimental water inlet temperature, T201, has been reproduced as a boundary condition in RELAP5 (in *TmdpVol-500*) during HX activation, from $t_3=1.86$ h to $t_5=7.6$ h; the simulated outlet temperature profile, in this time span, is in good agreement with the experimental value T202. Heat transfer coefficient relative to LBE flowing inside the FPS and HX, together with the value for the secondary water flowing in HX annular region, have been evaluated from RELAP5. Results, plotted in Figure 5.9, report, for assisted circulation regime, values of about 5000 and 3700 W/m²K respectively for FPS and HX; these values reduce to 3400 and 2400 W/m²K for natural circulation regime. For secondary water, a value of 1500 W/m²K is obtained; a peak is observed at the instant of HX activation due to the initial rapid vaporization of injected feedwater.

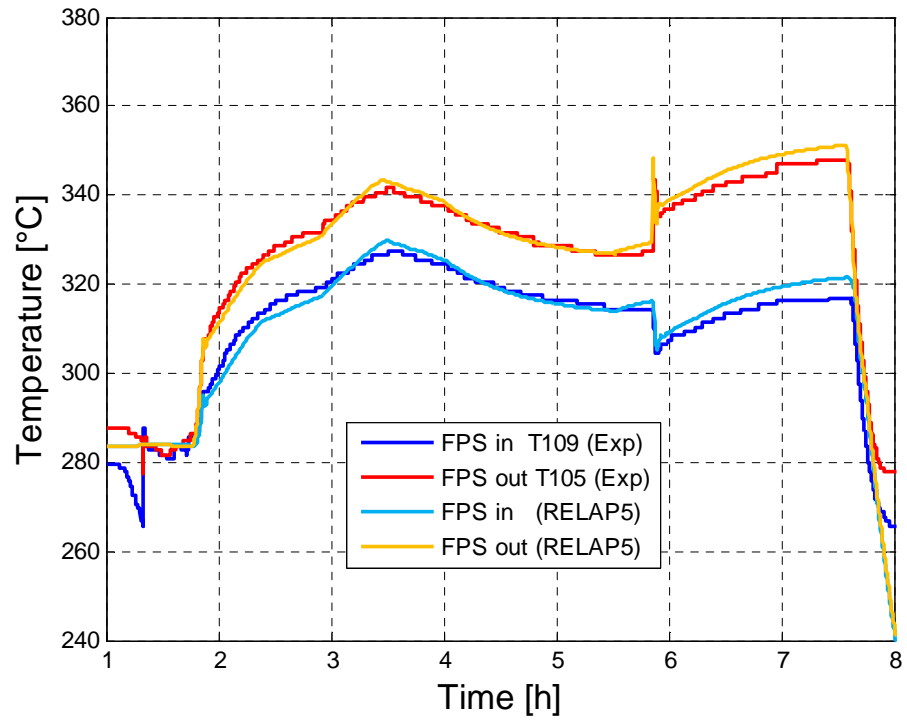


Figure 5.6: Comparison between measured and calculated inlet and outlet FPS temperatures

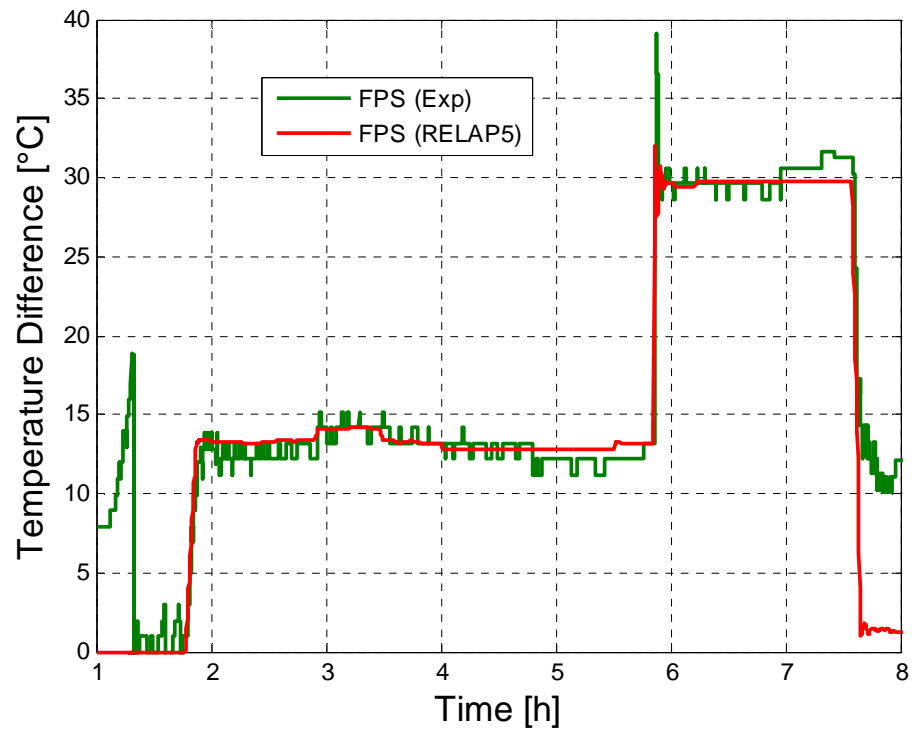


Figure 5.7: Comparison between measured and calculated FPS temperature difference

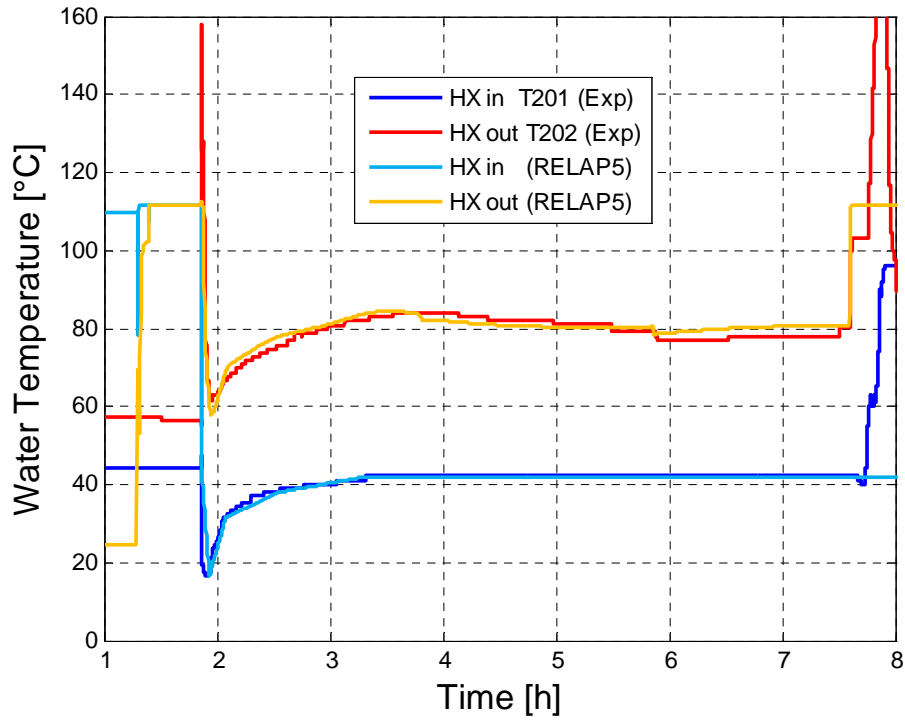


Figure 5.8: Comparison between measured and calculated inlet and outlet HX feedwater temperature

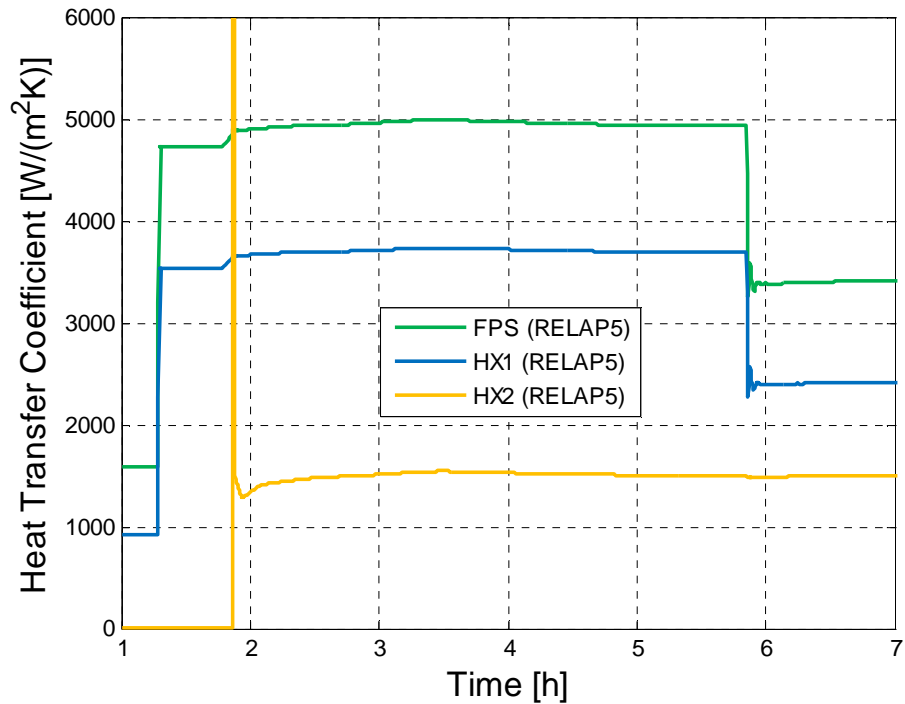


Figure 5.9: RELAP5 Heat Transfer Coefficient for LBE in FPS, HX primary side and for water in HX secondary side

Heat Exchanger double wall (see Figure 3.2) separating the descending *LBE* from ascending water has been modeled in RELAP5 by means of three consecutive cylindrical layer representing the inner tube wall (W1), the powder gap (GAP) and middle tube wall (W2), each subdivided in six mesh intervals. The two walls are made of AISI 304, while the gap consists of a stainless steel powder for which thermal conductivity equal to 10% of AISI 304 has been imposed. Figure 5.10 shows the temperature profile

along the double wall structure (at *HX* midplane) together with the fluids bulk temperatures. A comparison between assisted and natural circulation basically shows an overlapping of temperature profiles except for the *LBE* side bulk temperature which increases due to the lower heat transfer coefficient associated with the natural circulation regime. The powder gap (5.8 mm) represents the major contribute to the heat flux resistance with a temperature drop of about 180°C versus 25°C for the two walls (*W1+W2*), therefore, pointing out the importance in defining the thermal properties of the SS powder gap for the accuracy of model results.

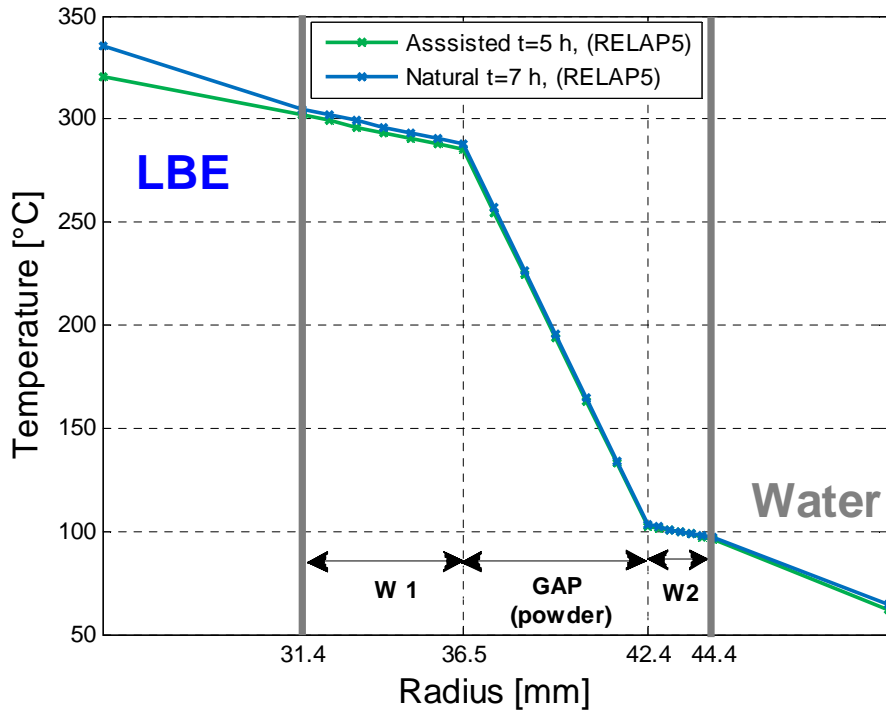


Figure 5.10: Temperature profile in HX double wall

The available driving force, during the assisted circulation phase, has been evaluated from RELAP5 results as follows:

$$\Delta P_{DF} = \Delta \rho \cdot g \cdot H_r \quad (5.1)$$

where H_r is the Riser height, set to 5.4 m, g gravity acceleration and $\Delta \rho$ is defined as:

$$\Delta \rho = \bar{\rho}_{LBE} - \rho_{r,TP} \quad (5.2)$$

and where $\bar{\rho}_{LBE}$ and $\rho_{r,TP}$ are respectively *LBE* mean density and two phase flow mean density inside the Riser; these values are directly supplied by the code. The obtained driving force, ΔP_{DF} , for the assisted circulation phase, is plotted in Figure 5.11 together with the mean riser void fraction, showing respectively values around 90 mbar and 1.65%.

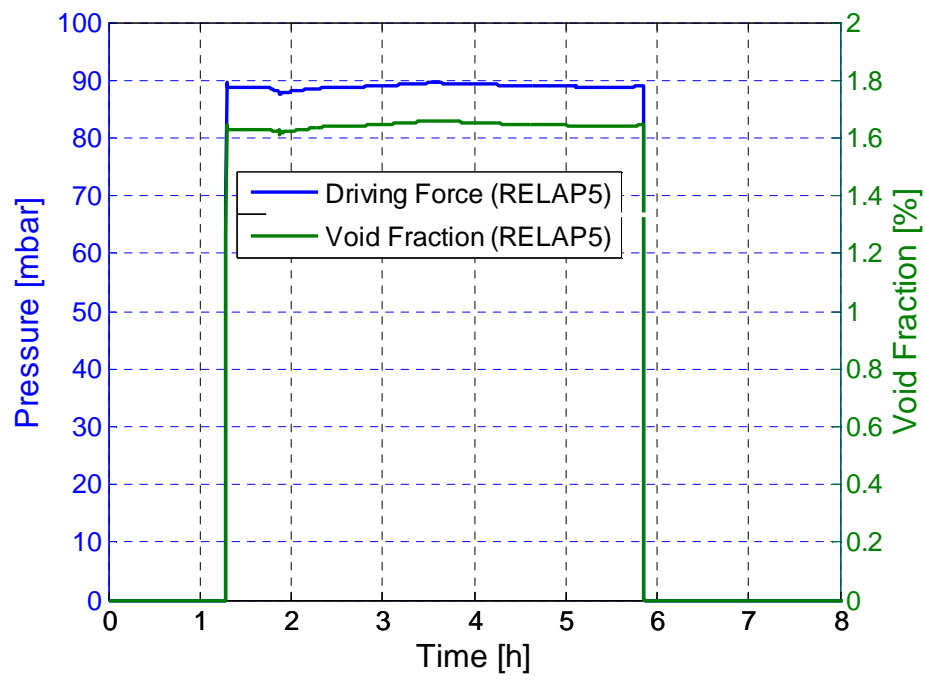


Figure 5.11: Driving force and void fraction in the riser

6. RELAP5-Fluent coupled calculations

In this section, the in house coupling tool [10] and the preliminary obtained results are presented and compared with those obtained from stand-alone RELAP5 [9] and with the experimental data as well. The set up numerical model is based on a two-way semi-implicit coupling scheme. The vertical part of the loop including the heater system and part of the piping before and after it, has been simulated by the Fluent [11] code both in a simplified 2D axial-symmetric configuration and in a 3D configuration, while the remaining part of the loop has been simulated by the RELAP5 code.

6.1 RELAP5 and Fluent models

Starting from the previous *NACIE* RELAP5 nodalization (see Figure 5.1), *NACIE* primary circuit was rearranged in such a way as to split the overall domain into two regions, one to be simulated by RELAP5 system code and one to be simulated using the Fluent *CFD* code (Non overlapping domains [12]). In particular the portion of the loop to be simulated by Fluent code is the Fuel Pin Simulator (*FPS*) of the loop (0.89 m see Figure 3.4) including a pipe of 0.21 m after it to reduce the possibility of occurrence of backflow conditions in the outlet section for the coupled code simulations, for an overall length of 1.1 m. In Figure 6.1 the RELAP5 nodalization used for the coupled simulations is reported. In *TmdpJun-115* and in *TmdpVol-112*, respectively, boundary conditions of mass flow rate and temperature obtained from an inner reference section of the Fluent domain are applied; while the pressure imposed *TmdpVol-110* is obtained from the inlet section of the *CFD* domain (see Figure 6.1). To reduce the occurrence of the previously mentioned backflow conditions in the outlet section of the *CFD* domain, a very high value of reverse form loss coefficient was set for the junction that connects *Pipe-210* to *Branch-100* and for the junction that connects *Branch-125* with *Pipe-130*.

Concerning the part of the domain of Fluent competence, it was firstly simulated as a simplified 2D axial symmetric domain and then as a 3D symmetric domain in order to reduce the computational effort.

The 2D axial symmetric *CFD* domain was discretized by a structured mesh composed by 7668 rectangular cells, uniformly distributed both in the axial and radial coordinates (see Figure 6.2). The 3D symmetric domain was schematized with the symmetry plane passing through the axis of the electric pins (not reproduced in the model), the pin bundle retaining rods are not reproduced in the model as well (see Figure 6.3). The three-dimensional domain was then discretized using 141045 hexahedral elements with refinements near the inlet and outlet sections in axial direction and near the electric pins wall along the radial direction (see Figure 6.4).

To model the *FPS* form loss coefficient a constant value of 3.5 has been considered. For this purpose five different interior faces have been set as a porous-jump in the 2D domain and in each of them an equivalent constant coefficient of concentrate pressure drop value of 0.7 was set. The same value of the form loss coefficient has been inserted in the *FPS* of the RELAP5 nodalization used for stand-alone calculations. Regarding the 3D simulation one interior face has been set as porous-jumps and an equivalent constant coefficient of concentrate pressure drop equal to 0.5 was set in order to introduce the pressure drop due to the spacers grid not simulated in the 3D geometrical domain.

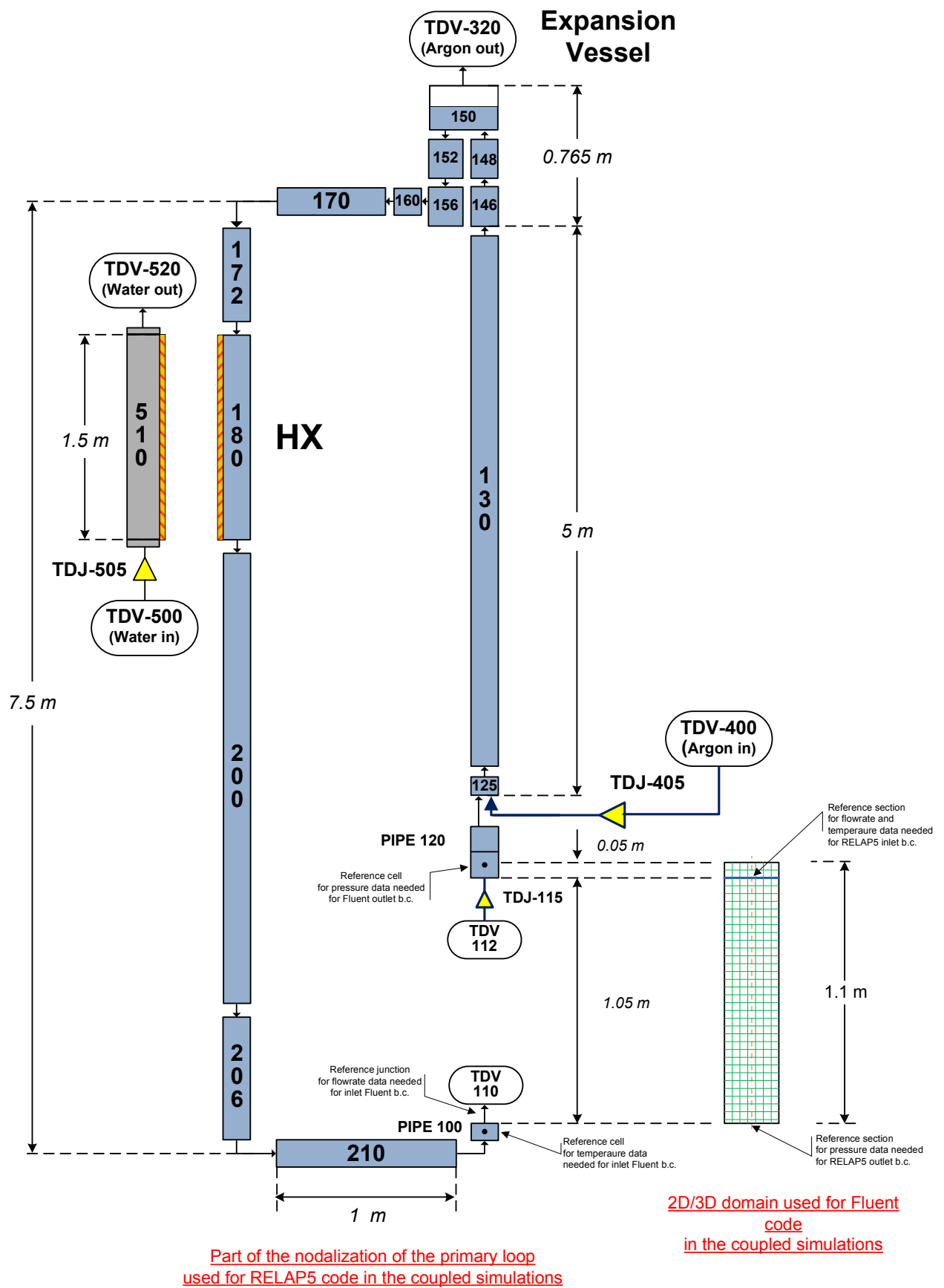


Figure 6.1: RELAP5 nodalization of the NACIE facility used for coupled simulation

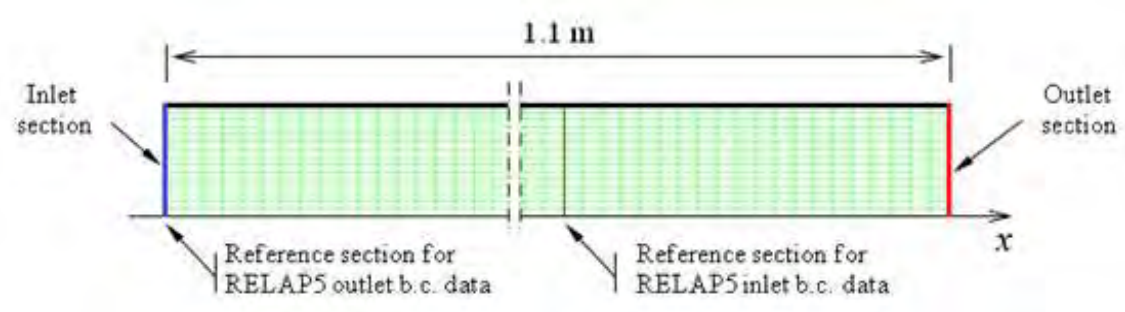


Figure 6.2: Axial-symmetric domain used in Fluent code for coupled simulations

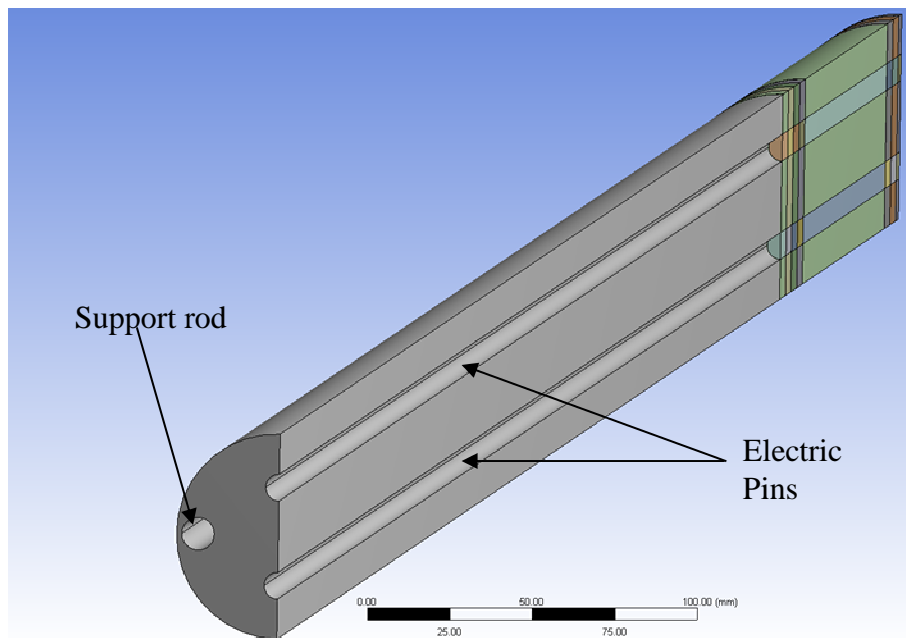


Figure 6.3: 3D domain used in Fluent code for coupled simulations

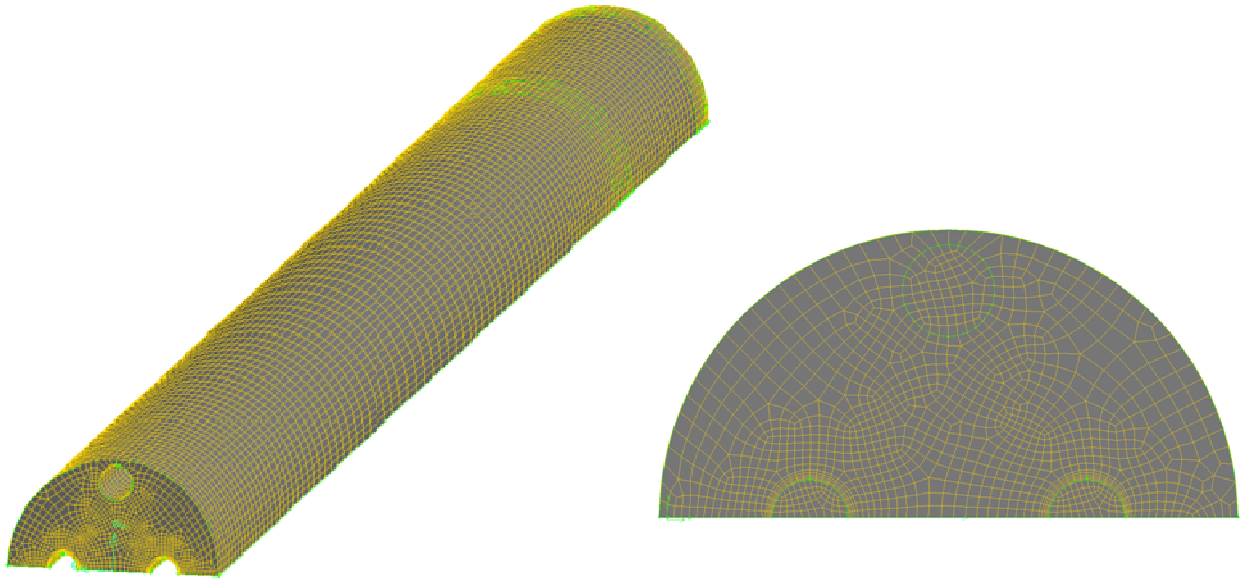


Figure 6.4: Spatial discretization of the 3D domain

For the coupled simulations, uniform temperature and mass flux have been imposed at the inlet section of the geometrical domain for 2D and 3D simulations as well. In addition, for the same inlet section, a fixed turbulence intensity of 7% and the hydraulic diameter are imposed as boundary conditions for the turbulence equations. The turbulence model adopted in the *CFD* calculations is the *RNG $k-\varepsilon$* , while the thermo-dynamic properties of the *LBE* are considered as a function of temperature in agreement with the properties equation reported in Section 1.

6.2 Coupling procedure

The scheme applied to the coupling procedure between RELAP5 and Fluent codes is shown in Figure 6.5 [10]. The execution of the RELAP5 code is operated by an appropriate MATLAB script, where a processing algorithm is also implemented to receive boundary conditions (b.c.) data from Fluent, at the beginning of the RELAP5 time step, and to send b.c. data to Fluent code, at the end of the RELAP5 time step. In addition, a special User Defined Function (*UDF*) was realized for Fluent code to receive b.c. data from RELAP5 and to send b.c. data to RELAP5 for each *CFD* time step.

An initial RELAP5 transient of 1000 s has been executed to reach steady state conditions with a uniform temperature of 237°C for Test 206 and 285°C for Test 306 respectively and with fluid at rest. The end of this initial transient was considered time zero from which the coupled simulation started. After that, a sequential explicit coupling calculation is activated, where the Fluent code (master code) advances firstly by one time step and then the RELAP5 code (slave code) advances for the same time step period, using data received from the master code.

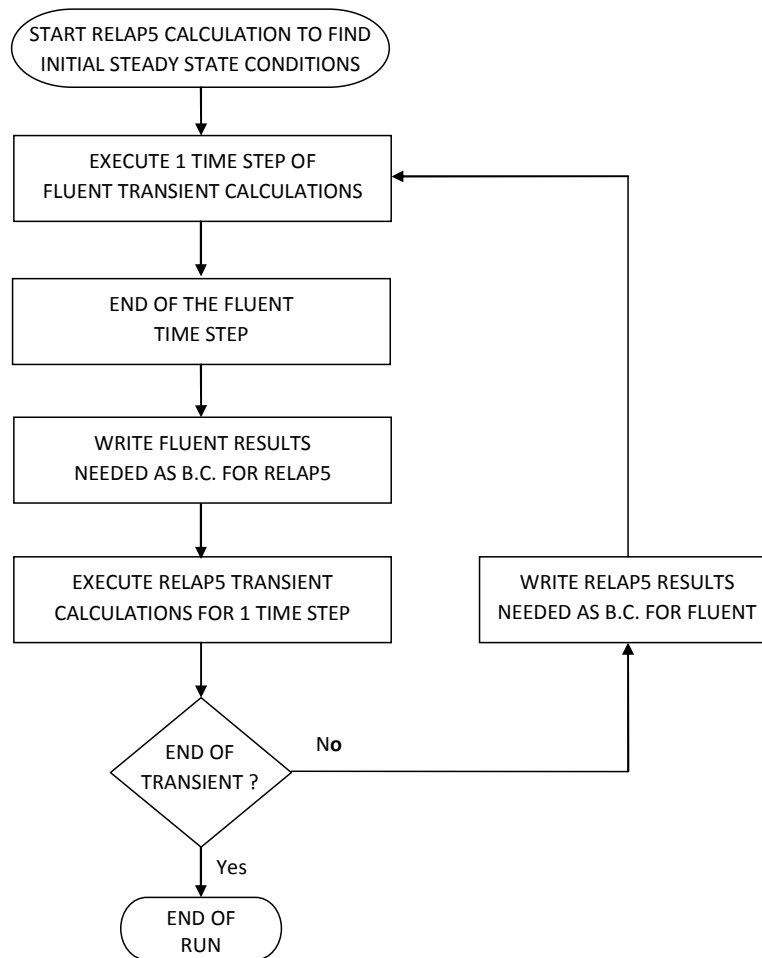


Figure 6.5: RELAP5-Fluent coupling procedure

6.3 Matrix of simulations

The performed simulations are representative of a gas enhanced circulation test. The experiment chosen as a reference test for numerical simulation are Test 206 and Test 306 reported in the previous Table 4.1. A total of five simulations have been performed, three for Test 206 and two for Test 306. In particular a RELAP5 stand alone simulation, a coupled simulation using a Fluent 2D axis symmetric domain and a coupled simulation using a Fluent 3D symmetric domain have been carried out for Test 206 while for Test 306 a RELAP5 stand alone simulation and a coupled simulation using a Fluent 2D axis symmetric domain for Test 306 were performed. The argon mass flow rate injected in the riser is increased linearly in the first 5 seconds of the transient for each step and then maintained constant according to the experimental time table. A preliminary sensitivity analysis showed that the time step needed to guaranty the convergence and independency of the results from the adopted time step itself is in the order of 0.005 s. Transient simulations with fixed time step have been carried out for an overall simulated transient of 27000 s.

The test matrix of the performed simulations is shown in Table 6.1 reporting adopted boundary conditions and main monitored variables.

Table 6.1: Matrix of performed simulations

Name	T_{av} [°C]	FPS Power %	Glift [Nl/min]	Monitored variables
Test 206	200-250	0	2,4,5,6,8, 10,6,5,4,3	LBE flow rate P_{in} and P_{out} in the HS
Test 306	300-350	0	2,4,5,6,8, 10,6,5,4,3	

6.4 Obtained results: Test 206 and Test 306

The LBE mass flow rate time trends obtained for Test 206 is reported in Figure 6.6, where the experimental results are compared with the calculated results both for the stand alone RELAP5 simulation and for the coupled RELAP5-Fluent 2D and 3D simulations.

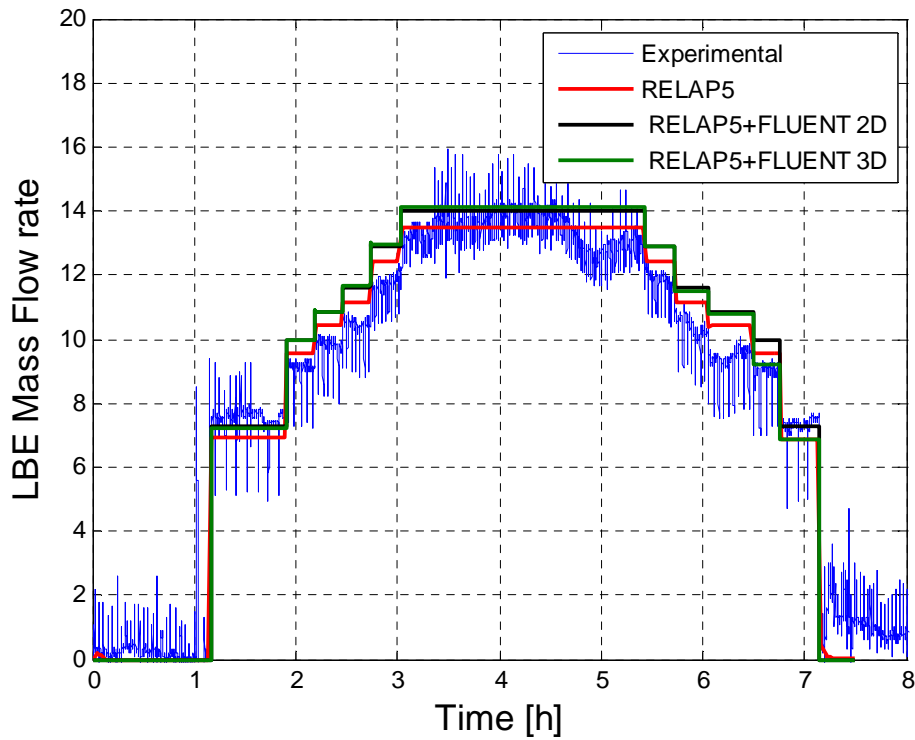


Figure 6.6: LBE mass flow rate results for Test 206

With respect to the experimental results, the calculated LBE mass flow rate overestimates them by less than 12%. Good agreement was found between the coupled code simulations with a 2D and 3D CFD domain, while the results of the coupled code simulations overestimate results obtained from the stand-alone RELAP5 by less than 5%.

Figure 6.7 shows the pressure difference between the FPS outlet and inlet section in Test 206. Good agreement was found between coupled and stand-alone RELAP5 results with a discrepancy that is lower than 1% between them.

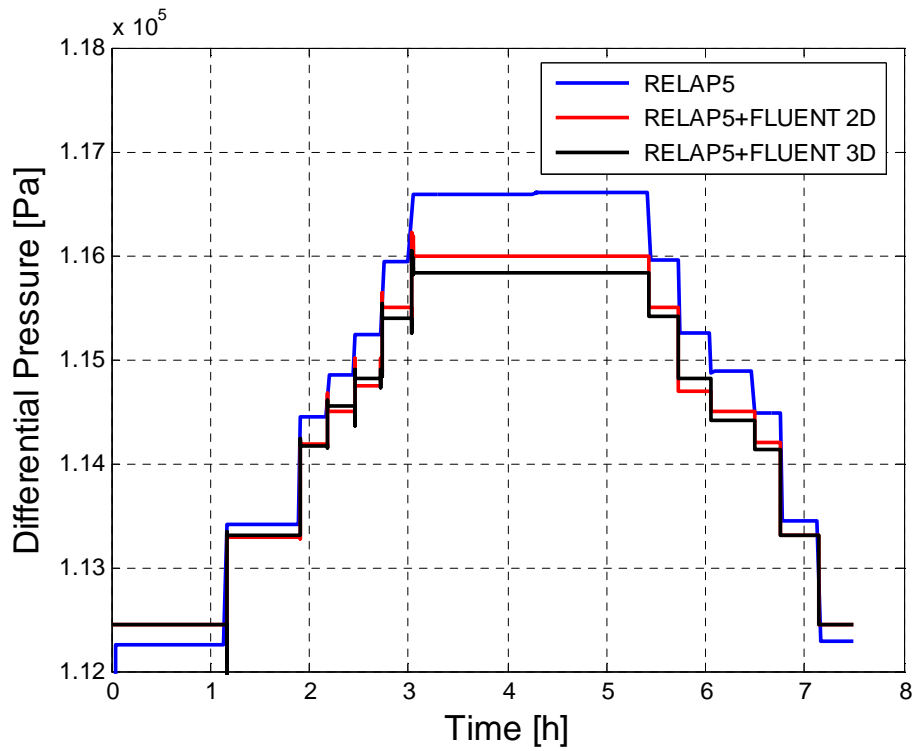


Figure 6.7: FPS pressure difference for Test 206

Figure 6.8 shows the pressure time trend at the inlet and outlet sections of the FPS. The calculated pressure by the coupled codes and by RELAP5 code on the FPS inlet and outlet sections, are practically the same as those evaluated by the stand-alone RELAP5 code with differences lower than 0.5%.

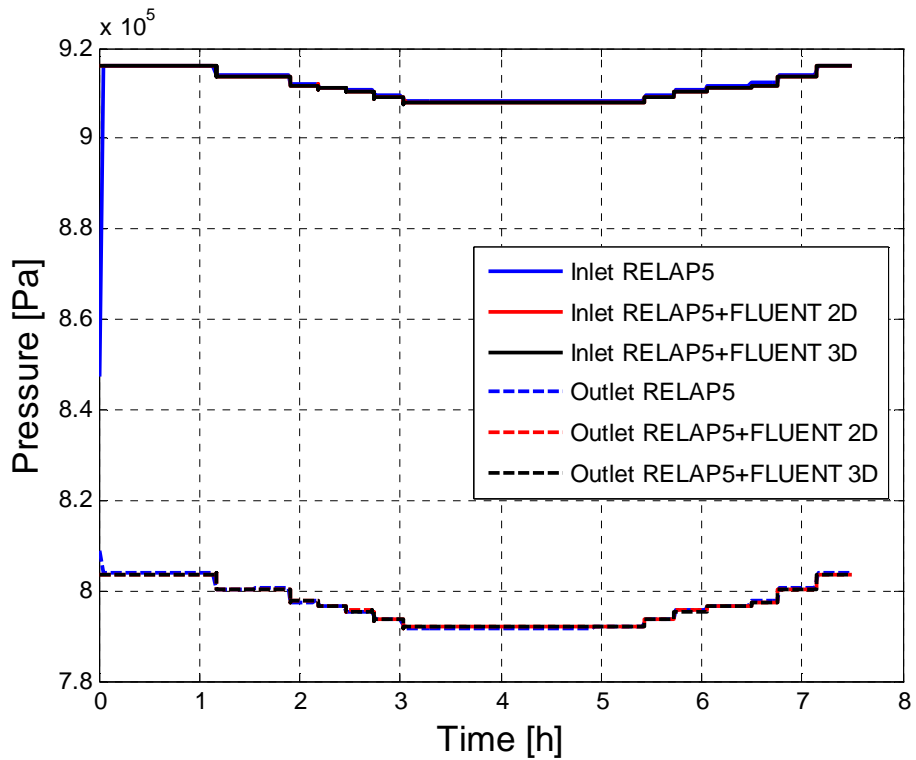


Figure 6.8: FPS inlet and outlet pressures for Test 206

In the following picture main results obtained from the coupled simulation with a 3D *CFD* geometrical domain are presented. In particular Figure 6.9 shows the pathlines colored by velocity along the vertical axis for $t = 3.5$ h (argon flow rate 10 NI/min), the picture refers to a plane section placed a $z = 0.89$ m in correspondence with the end of the loop bundle.

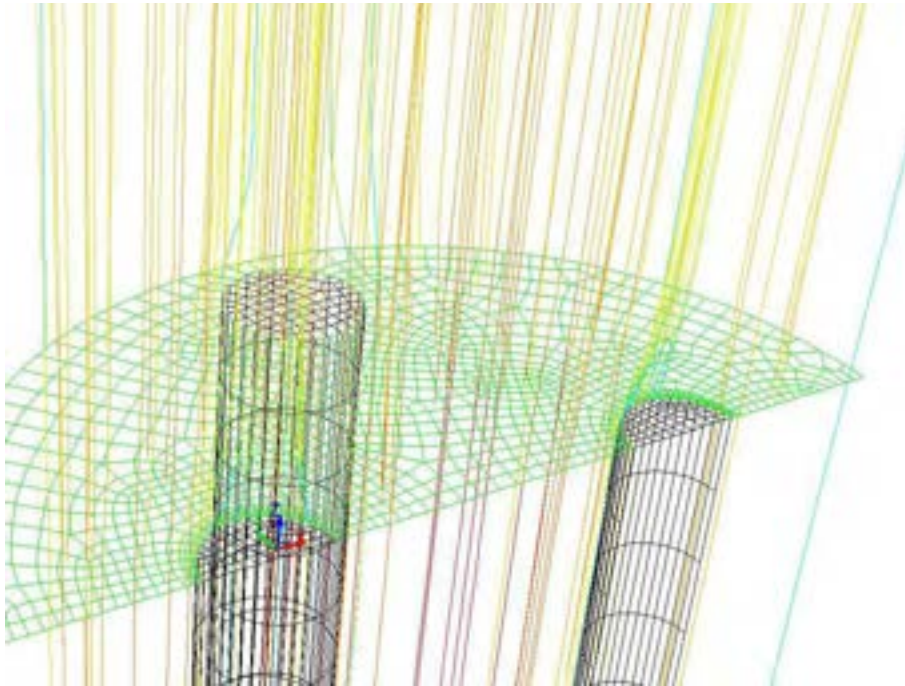


Figure 6.9: 3D *CFD* domain: pathlines at the exit of the pin bundle, Test 206

Figure 6.10 shows the vector velocity (w , along z -direction). The magnitude of w (area-weighted z velocity) predicted by the *CFD* code at the outlet section of the 3D geometrical domain is about 0.88 m/s ($t = 3.5$ h argon flow rate 10 NI/min).

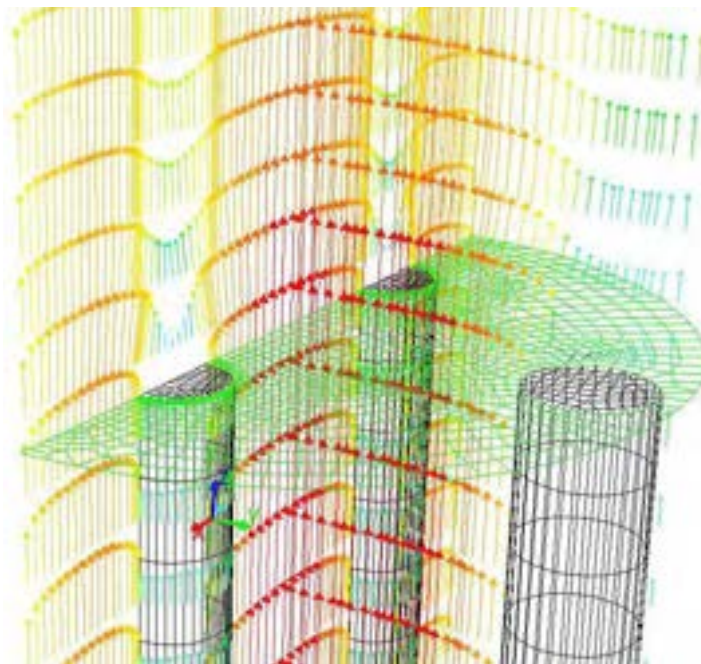


Figure 6.10: 3D *CFD* domain: vector velocity colored by z -velocity, Test 206

Figure 6.11 shows the distribution of turbulent kinetic energy k [m^2/s^2] for $t = 3.5$ h (argon flow rate 10 NL/min) in a section plane at $z = 0.89$ m and in a vertical plane passing through the axis of the supporting rod and vertical to the symmetry plane.

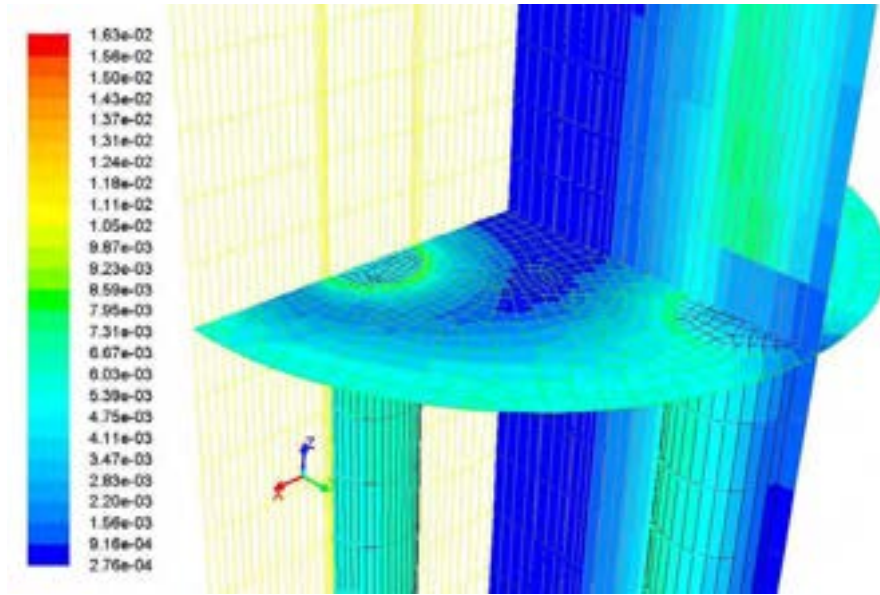


Figure 6.11: Distribution of turbulent kinetic energy k [m^2/s^2], Test 206

Figure 6.12 shows the LBE mass flow rate for Test 306. A good agreement is found between experimental results, those obtained from the stand-alone RELAP5 calculation and those obtained from the coupled simulation with 2D CFD domain. Maximum discrepancy between experimental and calculated results is less than 10%.

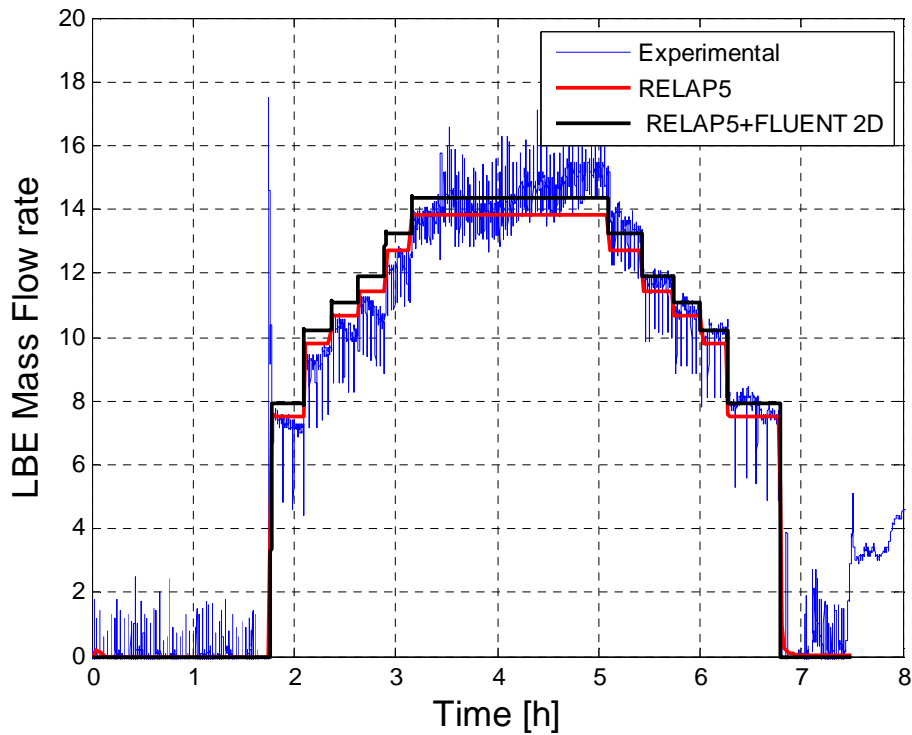


Figure 6.12: LBE mass flow rate results for Test 306

Figure 6.13 shows the pressure difference between the inlet and outlet section of the FPS. As it can be noted, the pressure drop in the FPS calculated by the Fluent code in the 2D coupled simulation fits well

with results obtained from stand-alone RELAP5 simulation showing a difference between them that is lower than 1%.

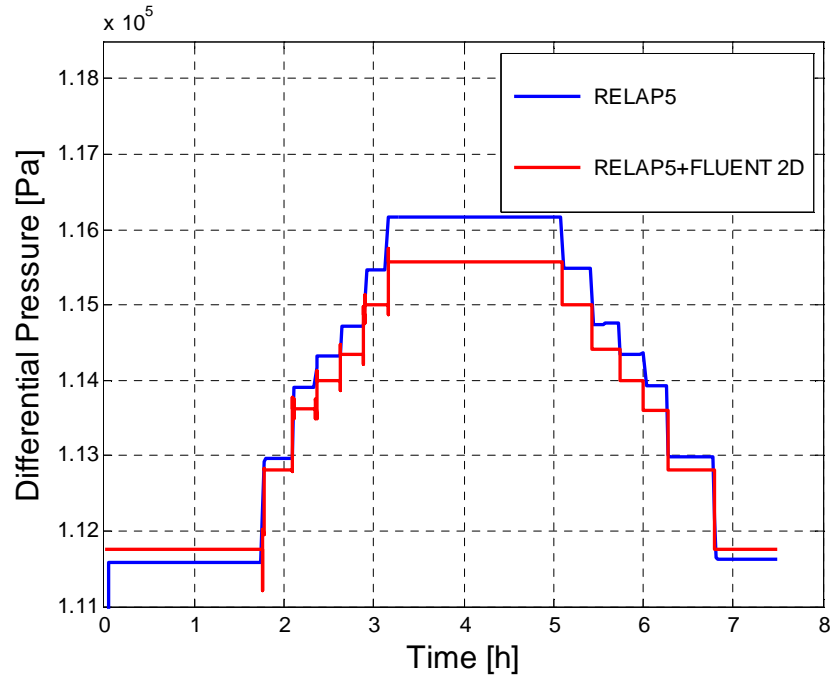


Figure 6.13: FPS pressure difference for Test 306

Figure 6.14 shows the pressure time trend at the inlet and outlet sections of the FPS for Test 306. The pressure calculated by the coupled codes on the FPS inlet and outlet section, are practically the same as those evaluated by the stand-alone RELAP5 code as observed for Test 206 with differences between them lower than 0.5%.

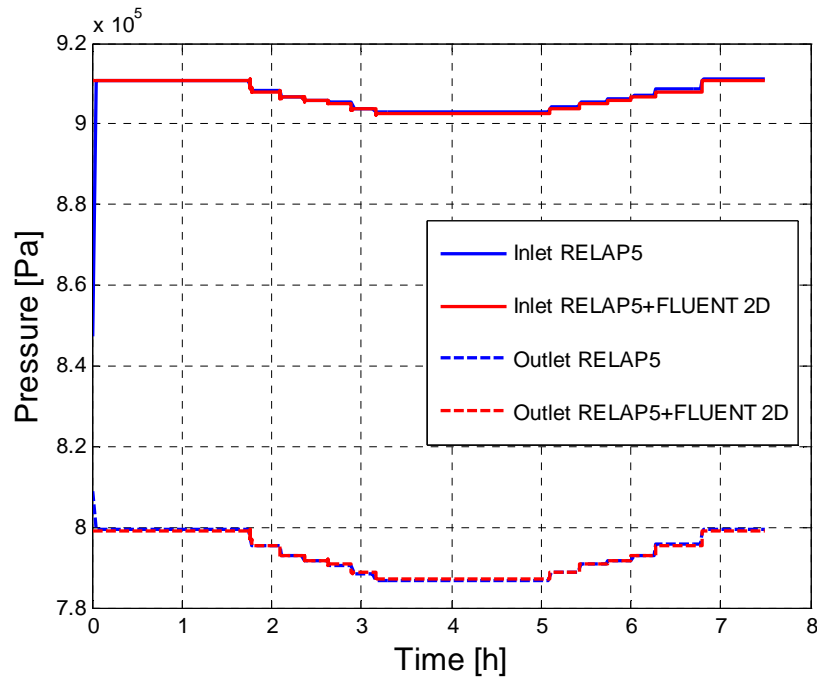


Figure 6.14: FPS Inlet and Outlet pressures for Test 306

Figure 6.15 summarizes results obtained for all the performed simulations. In particular, it shows calculated LBE mass flow rate versus experimental data for Test 206 and 306 for both stand-alone RELAP5 and coupled simulations. One can observe that calculated results satisfactorily predict the

experimental data with a trend that generally tend to overestimate the LBE mass flow rate obtained from the experimental campaign.

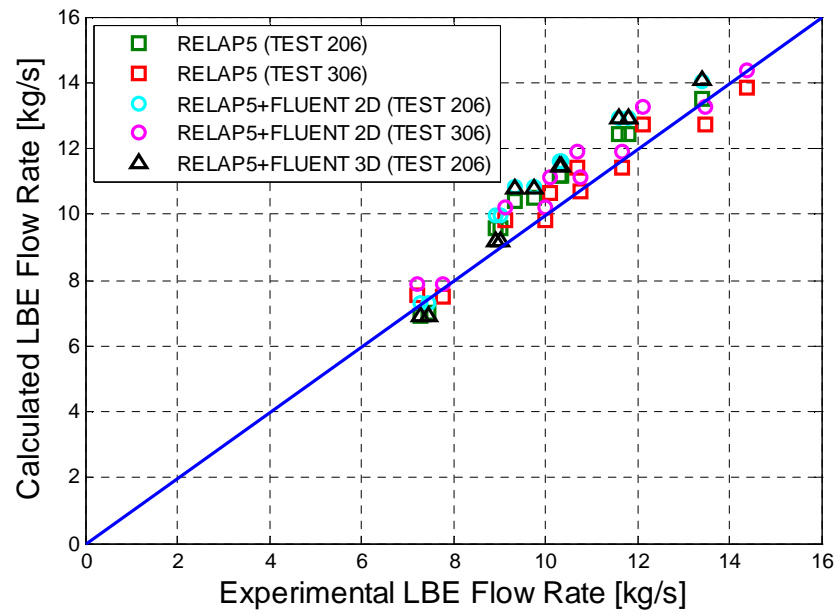


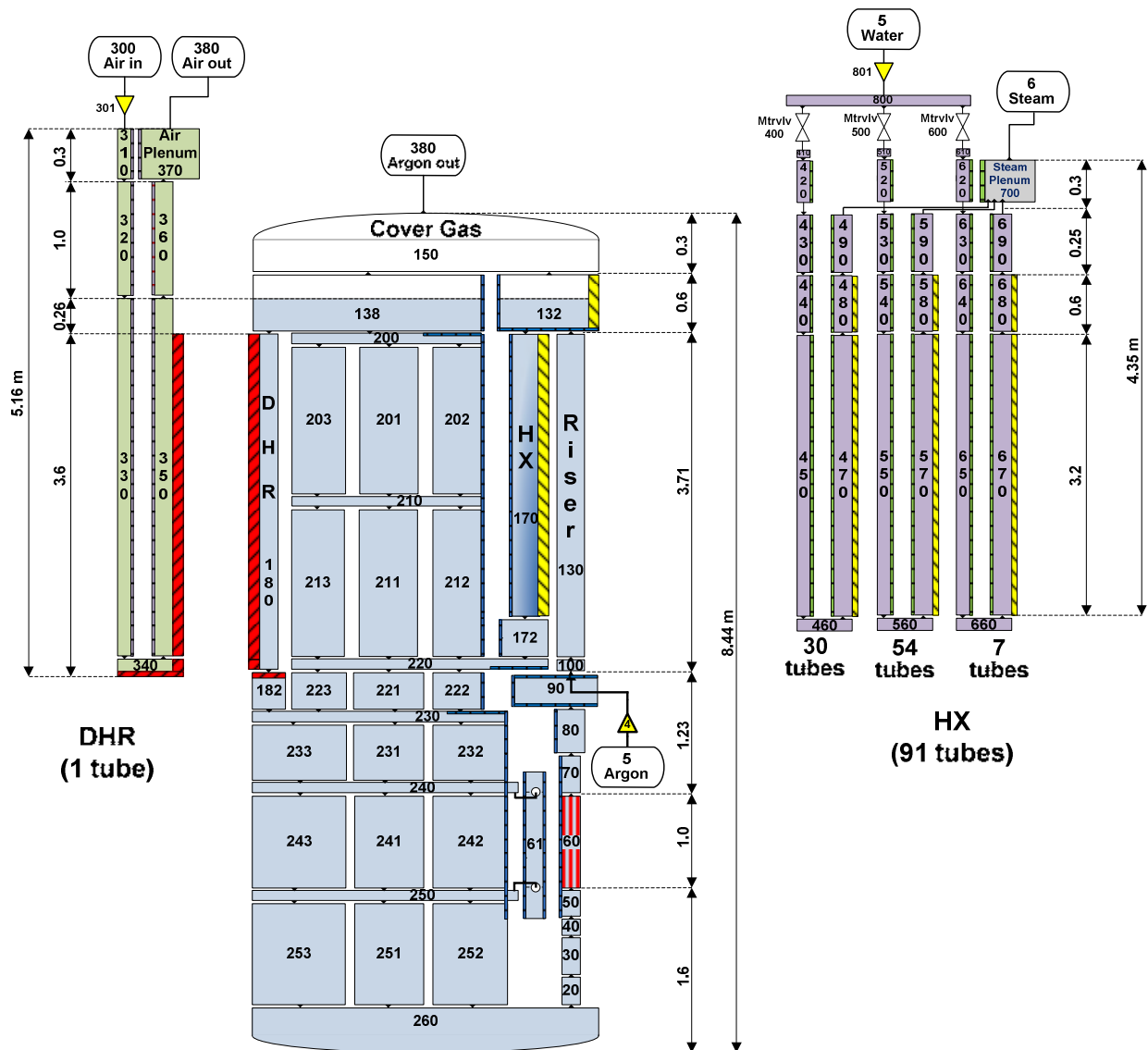
Figure 6.15: FPS Inlet and Outlet pressures for Test 306

7 Thermal-hydraulic post-test analysis of ICE-DHR

In order to assess the RELAP5 prediction capability for *LBE* pool type system, a post-test simulation was performed on *CIRCE* experimental campaign housing the upgraded *ICE* test section with a decay heat removal system (*DHR*). The reference experiment, Test IV, reproduces an accidental event characterized by a total loss of secondary circuit followed by reactor scram and *DHR* activation to remove the residual heat generation. The test is representative of a protected loss of heat sink scenario combined with primary circuit loss of flow (PLOH+LOF). The thermal hydraulic behavior of the system and the transition from forced to natural circulation were investigated.

7.1 Post-Test RELAP5 simulations

RELAP5 code [9] modified/implemented as described in Section 5 for *NACIE* simulation, was used to analyze the above described Test IV. The nodalization scheme adopted for *CIRCE* experiments simulations is depicted in Figure 7.1.



The upgraded configuration of *CIRCE-ICE* [13] test section was modeled. The main tank S100 contains about 69 tons of primary *LBE* with uniform initial temperature of 320°C; the liquid metal level is set to 0.26 m above the Riser outlet. The *LBE* enters into the aspiration duct from the pool bottom, reaching the Fuel Pin Simulator bundle (*FPS*), where it is heated (1 m active length, *Pipe-60*); it then flows upstream, crossing the fitting volume (*Pipe-90*), through the Riser (*Pipe-130*) and reaches the separator located in the upper part of the facility. A time dependent junction (*TmdpJun-4*) is connected to the Riser inlet (*Branch-100*) and injects argon (from *Tmdpvol-4*) to simulate the gas lift system during the assisted circulation phase. In the Separator (*Branch-132*), the gas is separated from the liquid metal and goes up in the vessel cover gas plenum (*Branch-150*), while the hot *LBE* goes downwards through the main Heat Exchanger (*HX*) shell (*Pipe-170*), to be cooled by the *HX* secondary water. The *LBE* exits flowing through a flow straightener (*Pipe-172*), placed in the lower part of the shell, into the downcomer. The pool external zone (*Pipe/Branch* from 200 to 260) was modeled by means of a series of parallel pipes connected by branches; such a nodalization of the pool, aims at improving the simulation of *LBE* mixing and thermal stratification phenomena observed experimentally.

The *DHR* primary side consists in an annular channel region modeled by *Pipe-180*. During the *DHR* activation, the hot *LBE* flows downwards from the pool top region (*Branch-138*) through the *DHR* primary side annular channel (*Pipe-180*). Here, *LBE* is cooled by the secondary side air flowing upstream through the *DHR* internal pipe, in a counter current heat exchanger configuration. The *LBE* cooled by the *DHR* exits in the pool through the *DHR* skirt (*Pipe-182*). Heat generation inside the *FPS* is simulated by an average heat structure representing the 37 electrical pins; the convective boundary condition is set according to Ushakov correlation [14] for rod bundle. Similarly, the same correlation is used for the *HX* primary side convective heat transfer with the 91 tubes. Heat transfer of *LBE* from the main flow-path to the quasi-stagnant *LBE* inside the pool was considered as well, with the exception of the Riser and the *DHR* shell which are thermally insulated, therefore considered adiabatic in the simulations. Heat dispersion of the *LBE* inside the tank towards the containment building was taken into account introducing an air convective heat transfer coefficient around $h_{ext}=1.5 \text{ W}/(\text{m}^2\text{K})$. Pressure losses along the main flow path were taken into account introducing concentrated pressure losses coefficients to simulate the presence of the Venturi nozzle (placed to measure the *LBE* flow) and the spacer grids.

The *HX* secondary side is modeled by three water loops, simulating the three compartments of 7 (inner), 54 (middle) and 30 (outer) bayonet tubes in which the *HX* bundle is arranged. Water is injected (*Tmdpjun-801*) inside each loop through three *Motor Valves*, flows downwards into the inner pipe and rises up through the annular region, where it exchanges heat in counter current with the primary *LBE*. Along the annular zone length, water begins to change its phase and the water/steam mixture is finally collected in the Steam Plenum (*Pipe-700*). The secondary side is thermally coupled with the primary side by means of an adequate heat structure between the water/steam mixture inside the annular zone and the *LBE* flowing through the tube bundles; a cylindrical double wall with helium inside the gap was modeled to compute the heat conduction. Vertical bundle without crossflow (with a $p/d=1.32$) convective condition type is set for the right boundary condition (*LBE* side), whereas the default convection condition is set for left boundary conditions (water/steam). A heat structure is foreseen to take into account the heat transfer between the cold water flowing in the inner tube and the water/steam mixture flowing through the annular zone. The bayonet tube of the *DHR* secondary side system is simulated according to design parameters. The air mass flow rate is imposed at the inner tube inlet section by means of a time dependent junction (*Tmdpjun-310*); air goes down towards the tube bottom plate and then flows upwards through the annular region up to the air Plenum located above the tank S100 cover. As for the *HX*, a heat structure provides the thermal coupling of the

primary and secondary fluids of the *DHR* system. Heat transferred between inner tube and annular region, is taken into account as well.

7.2 Test IV. Initial and Boundary Conditions

Test IV starts with *CIRCE* facility maintained at isothermal conditions (320°C) by means of heaters which compensate heat losses. In Figure 7.2 boundary conditions used for Test IV are illustrated.

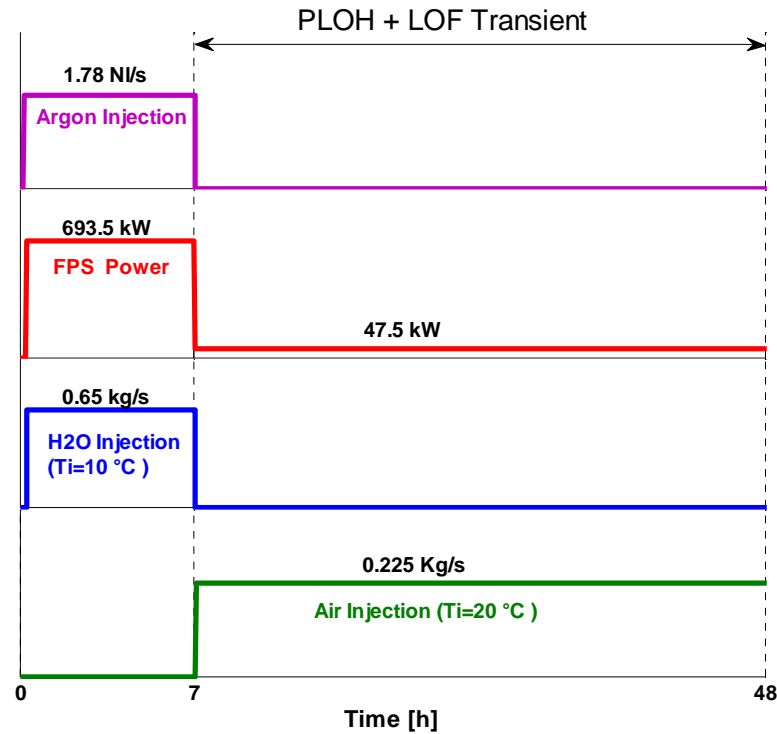


Figure 7.2: Boundary condition for Test IV

The RELAP5 simulation post-test analysis reproduces the experimental actions sequence performed during Test IV; the main boundary condition (*FPS* power, argon flow, and secondary fluid mass flow rates) are taken from the experimental outcomes. Namely, the simulation begins with the injection of argon (approximately 1.78 NI/s) inside the Riser to enhance primary *LBE* circulation. After reaching a stabilized value of the primary flow, power is supplied (power ramp) to the *FPS* up to a nominal value of 693.5 kW. Simultaneously, the main Heat Exchanger is activated by injecting 0.65 kg/s of water inside the 91 bayonet tubes in order to remove the supplied thermal power. This condition is maintained for several hours in order to attain a well stabilized condition in the primary system before beginning the transient phase. After about 7 hours from the beginning, the *PLOHS+LOF* transient is initialized performing the following procedures:

- i. switching off the gas injection (LOF);
- ii. rapidly reducing the *FPS* power down to 7% of the nominal value (47.5 kW) representative of the decay power level;
- iii. stopping the *HX* water injection;
- iv. starting the forced circulation of air (0.225 kg/s) in the secondary side *DHR* heat exchanger to remove the decay power.

The transient phase goes on for about 40 hours.

7.3 Test IV. *PLOH+LOF* Simulation Analysis

Post-test (Test IV) main outcomes of *PLOH+LOF* transient are compared with RELAP5 results. Figure from 7.3 to 7.6 show test boundary conditions (namely *FPS* Power, argon flow, *HX* feedwater and *DHR* air flow) and how they are reproduced in RELAP5 calculation. *FPS* Heat Power supply in RELAP5 simulation was reduced to 95% of measured electrical power (DC-KW) to account for the heat dissipation along the electrical cables to the *FPS*.

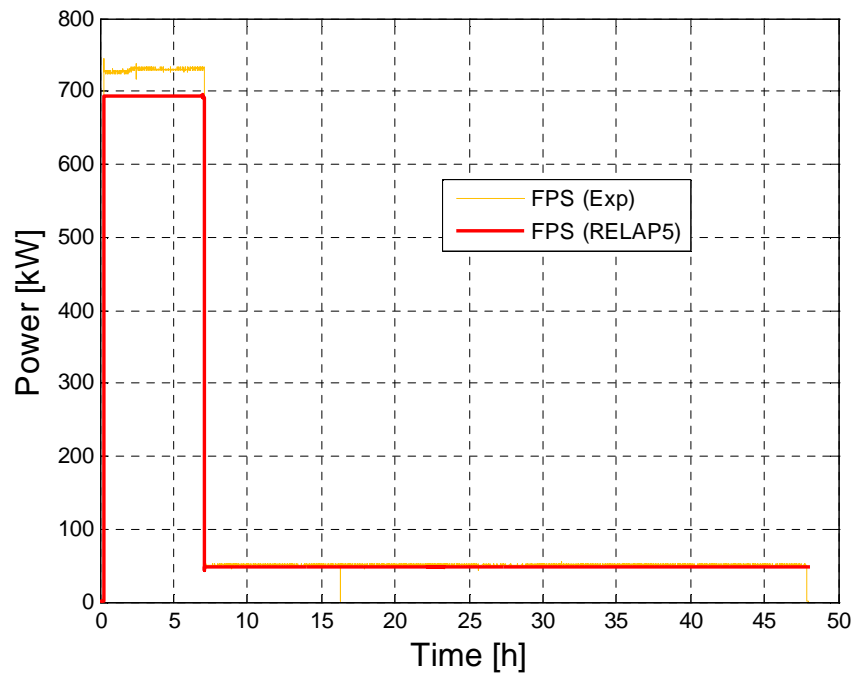


Figure 7.3: FPS Power

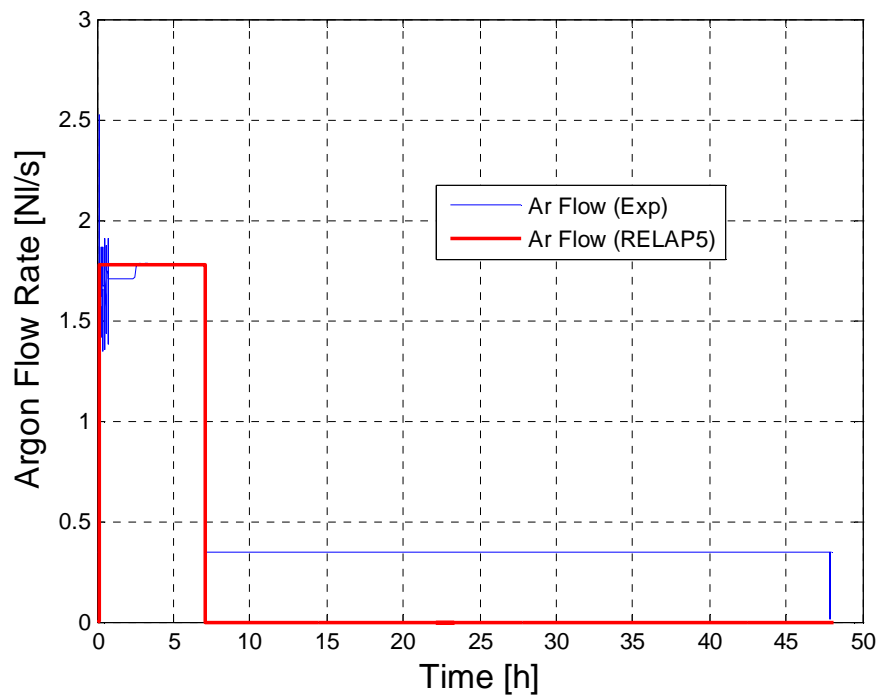


Figure 7.4: Argon Flow Rate

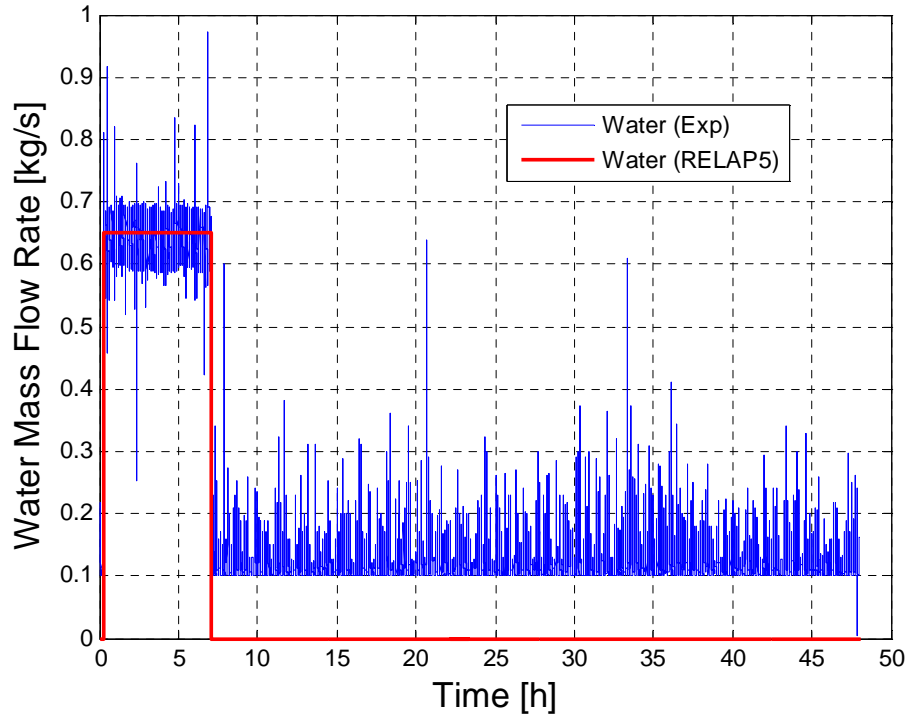


Figure 7.5: HX Water Mass Flow Rate

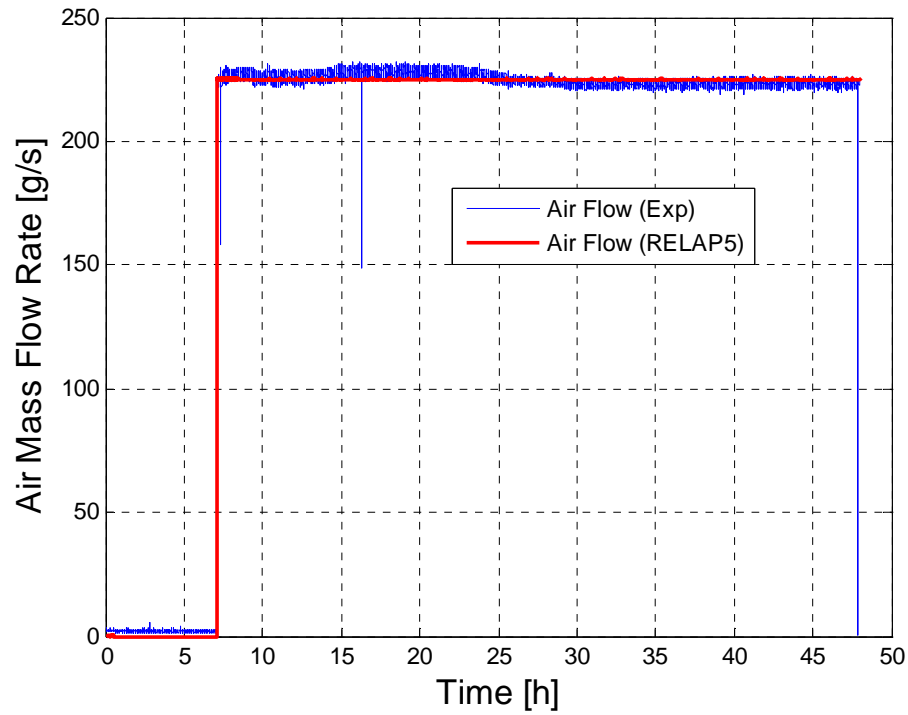


Figure 7.6: DHR Air Flow Rate

Pressure difference along the Riser is depicted in Figure 7.7, where experimental and RELAP5 results are compared. Good agreement is found during the assisted circulation phase, while a slight overestimation of simulated results are observed in natural circulation phase. Riser pressure difference is employed to obtain, by an indirect derivation [15], the average value of void fraction value along the Riser. This void fraction is adequately predicted by RELAP5 simulated results, as shown in Figure 7.8.

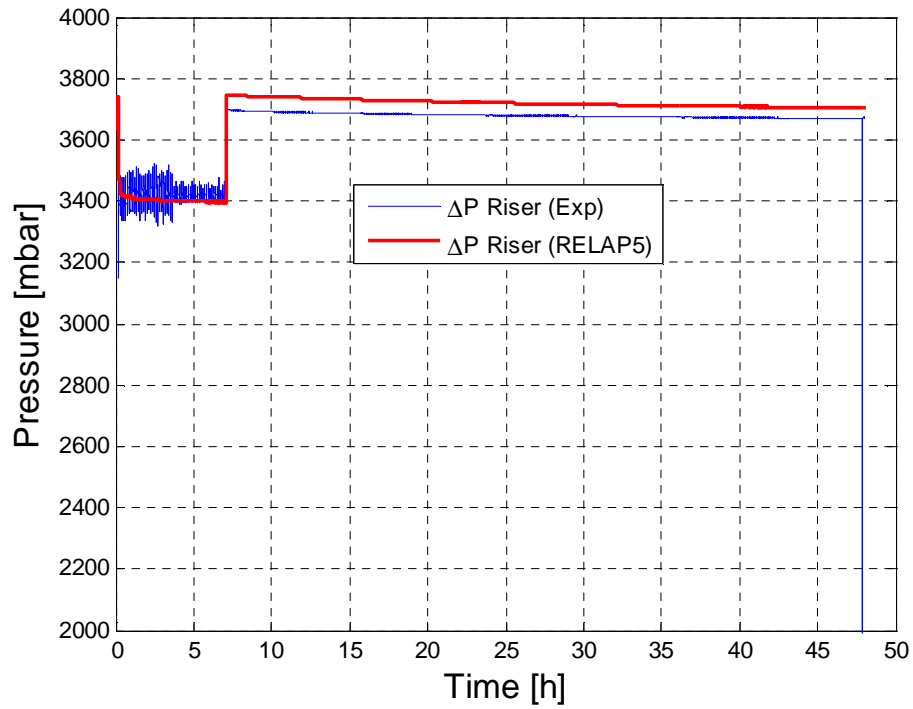


Figure 7.7: Pressure difference in the Riser

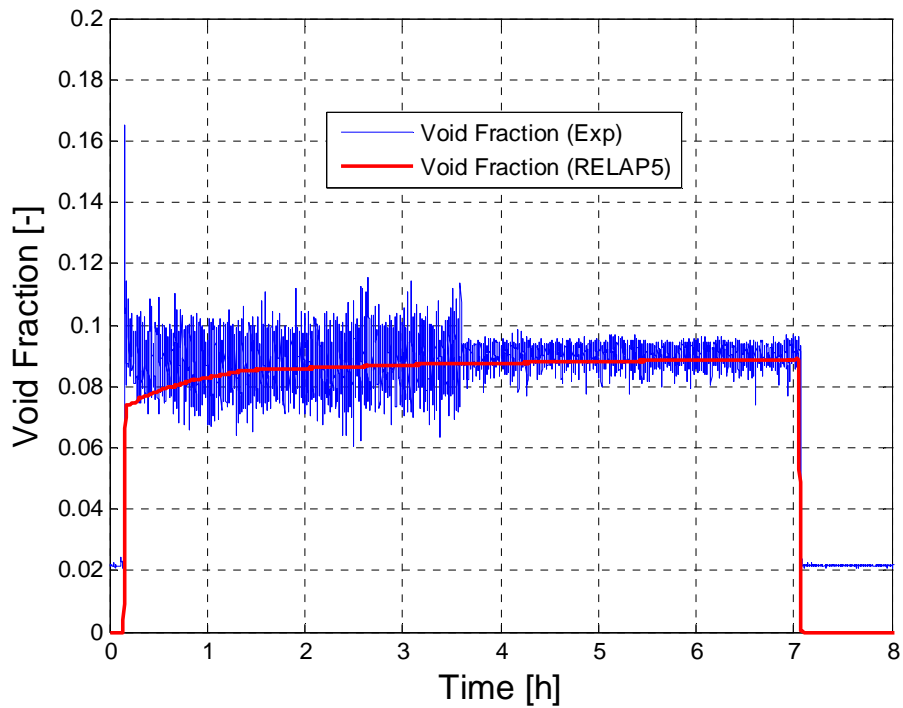


Figure 7.8: Average void fraction in the Riser

The available Driving Force , during the assisted circulation phase, was evaluated from RELAP5 results using eq.5.1 and eq.5.2, assuming a Riser height, H_r , equal to 3.7 m; results obtained by the code are plotted in Figure 7.9 and give a final value to around 325 mbar.

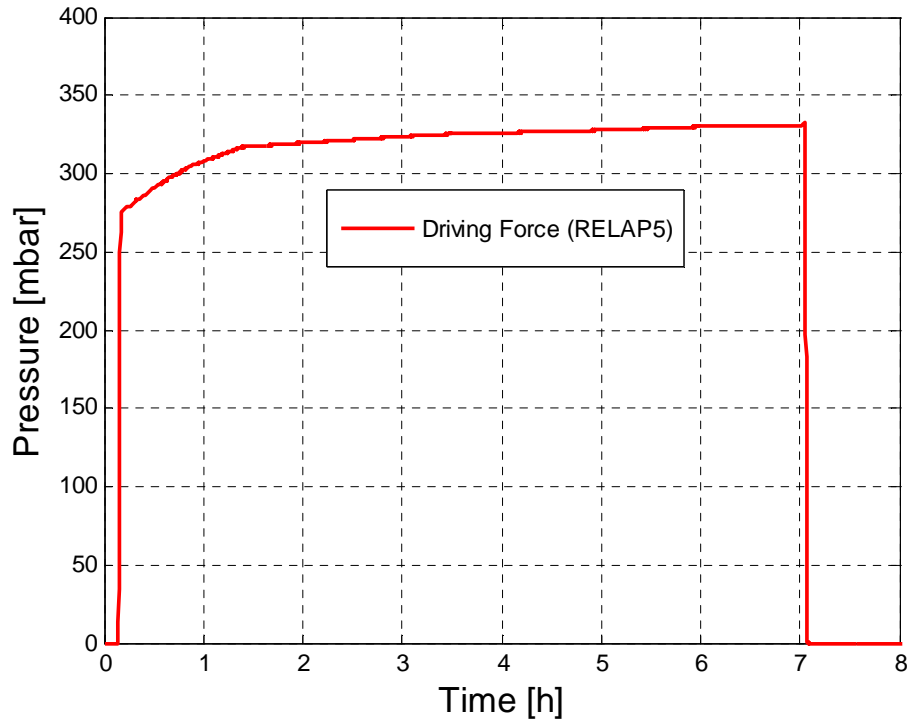


Figure 7.9: Driving force available for LBE circulation

Measured and simulated values of *LBE* mass flow rate along *CIRCE* facility main flow path are compared in Figure 10, showing good agreement both in forced and natural circulation regimes. The value of the mass flow rate through *DHR* predicted by the code is reported as well. During assisted circulation (first 7 h) *LBE* mass flow rate, measured in the *FPS*, is characterized by wide oscillation with an average value of 56.5 kg/s which is adequately reproduced by the code. As soon as *PLOH+LOF* transient initiates, at about 7 h, stable natural circulation in the primary circuit is established; measured and simulated values are about 7.2 and 7.7 kg/s, respectively. The predicted *DHR* mass flow rate shows a progressive increase, and stabilizes at 6.9 kg/s at about 9 h. Experimental inlet and outlet *FPS* temperature time trends during the test are shown in Figure 11 and compared to RELAP5 results. The code satisfactorily simulates the temperature trend related to the full power assisted circulation phase during the first 7 h, reaching a stationary values of about 370 and 284°C for *FPS* outlet and inlet temperatures, respectively. The onset of natural circulation and power reduction (about 7 % of nominal power) following the *PLOH+LOF* event, produces a sudden drop of the previous *FPS* temperatures to 322 and 280°C. From those values, temperatures increase till the end of the test ($t=48$ h) without reaching a stationary condition. The trend obtained by the code during this transient is similar to the experimental one, however it presents some discrepancies probably ascribed to some uncertainties in defining the *DHR* system efficiency as well as the evaluation of the facility heat losses towards the environment.

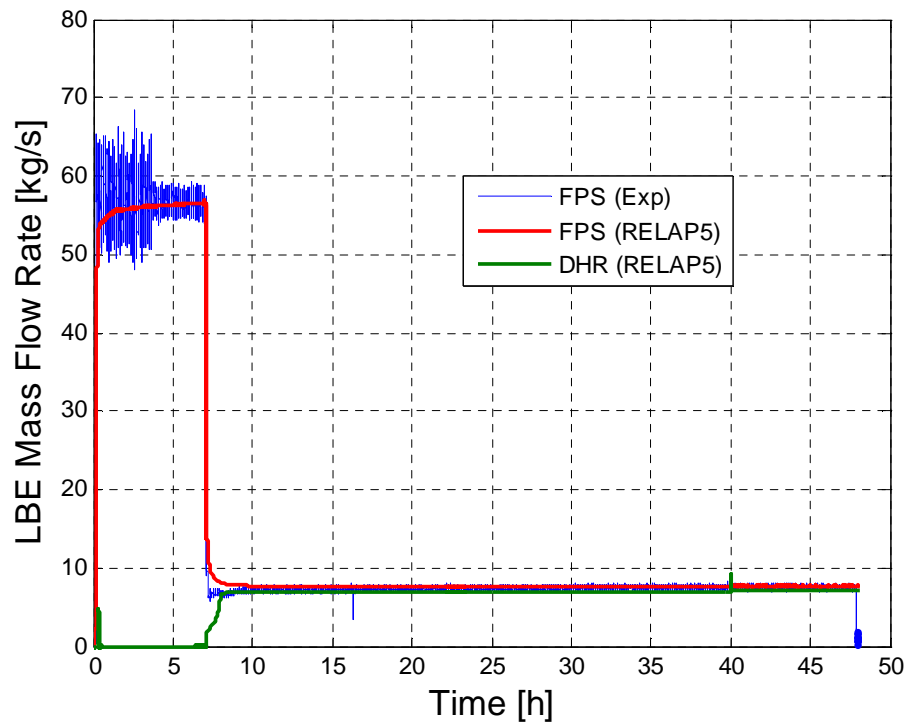


Figure 7.10: FPS and DHR mass flow rate

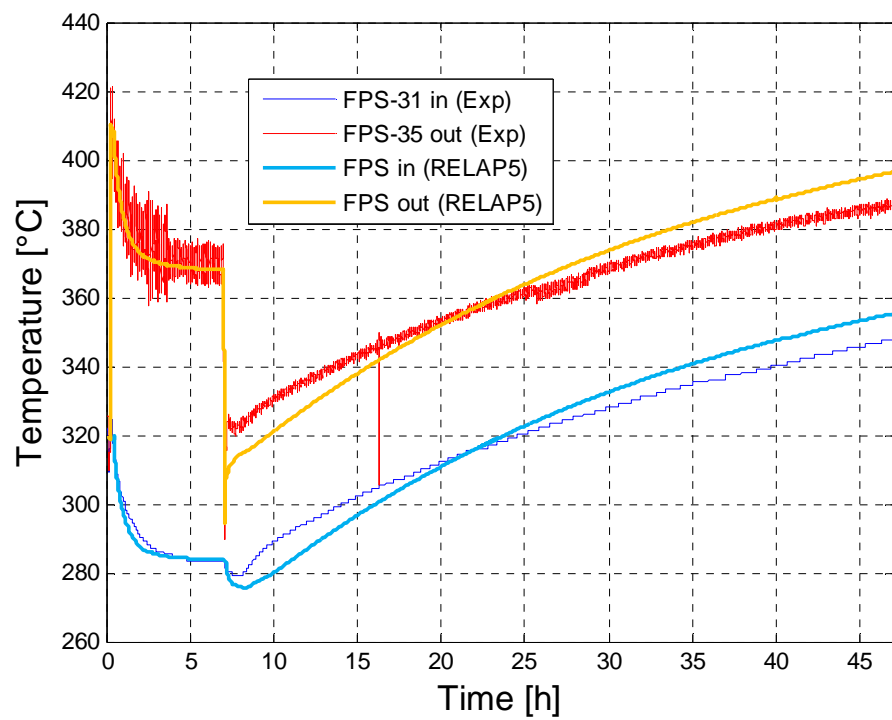


Figure 7.11: FPS inlet and outlet temperatures

8. Conclusions

In this work carried out at the *DICI* (Dipartimento di Ingegneria Civile e Industriale) of Pisa University in collaboration with *ENEA* Brasimone Research Centre, the mathematical relations used by the RELAP5 system code to generate the table of *LBE*, Lead and Sodium, were modified according to V. Sobolev's work. In order to assess the performed modifications, post-test simulations were carried out and the obtained results were compared to the experimental ones.

The post-test simulation performed using RELAP5/Mod3.3 with the newly implemented features, proved the reliability of the code in predicting experimental results of *LBE* thermal hydraulic behavior for the two facilities under investigation, *NACIE* and *CIRCE*, both in assisted and natural circulation regimes. The validity of the code model in simulating *CIRCE-DHR* pool experiment representative of a *PLOH+LOF* transient is demonstrated by RELAP5 post-analysis comparison. *LBE* primary flow is adequately reproduced in both assisted and natural circulation conditions, including the transition from one regime to the other. Likewise the values of the pressure difference and gas void fraction inside the Riser are well predicted. The model properly simulates *HX* power removal and the attainment of stabilized conditions during full power run, whereas some discrepancies remain in the simulation of transient conditions characterized by reduced power supply and the *DHR* system activation.

Furthermore, the *NACIE* loop configuration during a loss of flow experiment is well simulated by the code for what concerns *LBE* flow rate and temperature evolution, before and after the simulated incidental event (*ULOF*). Quantification of heat losses to the environment reveals to be a non negligible issue for temperature evolution prediction of the examined systems, especially for low power experiments.

The *NACIE* model, experimentally validated, was then modified in order to be applied to coupled simulations using RELAP5 system code and Fluent *CFD* code. The set up numerical model is based on a two-way semi-implicit coupling scheme and axialsymmetric 2D and 3D geometrical *CFD* domains were investigated. The developed coupling method proved its capability in the simulation of the thermal-hydraulic behaviour of an experimental facility like *NACIE*. Two experimental tests characterized by gas enhanced circulation with different gas flow rate injections (2-4-5-6-8-10 NI/min) were simulated and obtained results for *LBE* mass flow rate showed good agreement with the experimental data, moreover good agreement was found for the differential pressure between the inlet and outlet section of the *FPS* computed by stand alone RELAP5 and coupled simulations.

Further work must be done to optimize the numerical algorithm and to improve numerical stability. In particular, efforts must be carried out to develop an implicit scheme and to parallelize the coupled methodology in order to reduce computational time.

References

- [1] Sobolev, "Database of thermophysical properties of liquid metal coolants for GEN-IV", November 2010 (rev. Dec. 2011), SCK-CEN, Belgium.
- [2] R.A. Seban, T. T. Shimazaki, "Heat transfer to a fluid flowing turbulently in a smooth pipe with walls at constant temperature", Transactions of the ASME, Vol. 73, pp. 803-809, 1951.
- [3] X. Cheng e N. Tak, "Investigation on Turbulent Heat Transfer to Lead-Bismuth Eutectic Flows in Circular Tubes for Nuclear Application", Nuclear Engineering and Design, Vol. 236, pp 1874-2885, 2006.
- [4] P.A. Ushakov, A. V. Zhukov, N. M. Matyukhin, "Heat transfer to liquid metals in regular arrays of fuel elements", High temperature, Vol.15, pp. 868-873, 1977.
- [5] K. Mikityuk, "Heat Transfer to Liquid Metal: Data and Correlation for Tube Bundles", Nuclear Engineering and Design, Vol. 239, pp 680-687, 2009.
- [6] G.Coccoluto, P.Gaggini, V. Labanti, M.Tarantino, W. Ambrosini, N. Forgione, A. Napoli, F. Oriolo, "*Heavy liquid metal natural circulation in a one-dimensional loop*", Nuclear Engineering and Design 24 (2011), 1301-1309.
- [7] M.Tarantino, D. Benardi, G.Coccoluto, P.Gaggini, V. Labanti, N. Forgione, A. Napoli "*Natural and gas Enhanced circulation test in the NACIE Heavy Liquid Metal Loop*", proceedings of ICONE, 18th International Conference on Nuclear Engineering, May 17-21,Xi'an, China
- [8] I.Di Piazza, D. Martelli, Report *ENEA NA-T-R-029,"Experimental circulation tests on a prototypical inductive flow meter with the NACIE loop"*, 2013
- [9] Relap5/Mod.3.3 Code Manual, Volume II. Appendix A: Input Requirements, Nuclear Safety Analysis Division, January 2003.
- [10] G. Barone, N. Forgione, D. Martelli, A. Del Nevo, Report *ENEA LP3.C4 AdP MSE-ENEA, "Pre-test analysis of thermal-hydraulic behavior of the NACIE facility for the characterization of a fuel pin bundle"*, 2012
- [11] ANSYS® Academic Research, Release 14.0, Help System, Ansys Fluent 14.0 User's Guide, ANSYS, Inc.
- [12] L. Mengali, M. Lanfredini, F. Moretti, F. D'Auria, Report *ENEA LP3.C1.C AdP MSE-ENEA, "Stato dell'arte sull' accoppiamento fra codici di sistema e di fluidodinamica computazionale. Applicazione generale su sistemi a metallo liquido pesante"*, 2012
- [13] D. Martelli, N. Forgione, "*CIRCE Experimental Report*", Università di Pisa, Dipartimento di Ingegneria Civile e Industriale,DICI RL23 (May 2013).
- [14] P.A. Ushakov, A. V. Zhukov, N. M. Matyukhin, "*Heat transfer to liquid metals in regular arrays of fuel elements*", High temperature, Vol.15, pp. 868-873, 1977.
- [15] Tarantino M., Report *ENEA HS-F-R-001 "Gas Enhanced Circulation Experiments On Heavy Liquid Metal System"*, 2007.

Nomenclature

Roman letters

a_i	coefficient [-]
b_i	coefficient [-]
c_p	specific heat capacity at constant pressure [J/(kg K)]
c_v	specific heat capacity at constant volume [J/(kg K)]
d_i	coefficient [-]
D	pin diameter [m]
e_i	coefficient [-]
g	gravity acceleration [m/s ²]
h^{ext}	external heat transfer coefficient [W/(m ² K)]
h	specific enthalpy [J/kg]
H	thermal centers elevation [m]
H_r	Riser height
k	thermal conductivity [W/(m K)]
Nu	Nusselt number [-]
ρ	pitch [m]
P	pressure [Pa]
P_{ref}	reference pressure [Pa]
P_{sat}	saturation pressure [Pa]
R	gas constant [J/(kg k)]
r_i	coefficient [-]
s	specific entropy [J/(kg k)]
T	temperature [°C]
T_{sat}	saturation temperature [°C]
u	specific internal energy [J/kg]
w_s	sound speed [m/s]
w	<i>z-velocity</i> [m/s]
W	Pipe thickness [mm]

Greek letters

β	volumetric thermal expansion coefficient [K ⁻¹]
μ	dynamic viscosity [Pa s]

ν	specific volume [m^3/kg]
κ	isothermal coefficient of compressibility [m^2/N]
ρ	density [kg/m^3]
ε	turbulent kinetic energy dissipation [m^2/s^3]

Abbreviations and acronyms

<i>b.c.</i>	Boundary Conditions
<i>CFD</i>	Computational Fluid Dynamic
<i>CIRCE</i>	Circolazione Eutettico
<i>DHR</i>	Decay heat removal system
<i>DF</i>	Driving Force
<i>DICI</i>	Dipartimento di Ingegneria Civile e Industriale
<i>ENEA</i> sostenibile	Agenzia nazionale per le nuove tecnologie, l'energia e lo sviluppo economico sostenibile
<i>EOS</i>	Equation Of State
<i>FC</i>	Forced Circulation
<i>FPS</i>	Fuel Pin Simulator
<i>ICE</i>	Integral Circulation Experiment
<i>HLM</i>	Heavy liquid metal
<i>HX</i>	Heat Exchanger
<i>LBE</i>	Lead bismuth eutectic
<i>LMs</i>	Liquid Metals
<i>LOF</i>	Loss Of Flow
<i>NACIE</i>	Natural Circulation Experiment
<i>NC</i>	Natural Circulation
<i>NPS</i>	Nominal Pipe Size
<i>PLOH</i>	Protected Loss Of Heat Sink
<i>RELAP</i>	Reactor Loss of Coolant Analysis Program
<i>RNG</i>	<i>Renormalization Group Model</i>
<i>SI</i>	Système international d'unités
<i>SS</i>	Stainless Steel
<i>UDF</i>	User Defined Function
<i>ULOF</i>	Unprotected Loss Of Flow

Breve CV del gruppo di lavoro

Gianluca Barone

Si è laureato in Ingegnere Nucleare all'Università di Roma nel 2004 ed ha conseguito il Master di II livello in "Tecnologie degli Impianti Nucleari" presso l'Università di Pisa nel 2011. Attualmente borsista presso il DIMNP dell'Università di Pisa. Esperto di codici di sistema, con particolare riguardo al codice di termoidraulica nucleare RELAP5.

Nicola Forgione

Ricercatore in Impianti Nucleari presso il Dipartimento di ingegneria Meccanica, Nucleare e della Produzione (DIMNP) dell'Università di Pisa dal 20 dicembre 2007. Laureato in Ingegneria Nucleare nel 1996 presso l'Università di Pisa ed in possesso del titolo di Dottore di Ricerca in Sicurezza degli Impianti Nucleari conseguito all'Università di Pisa nel 2000. La sua attività di ricerca è incentrata principalmente sulla termofluidodinamica degli impianti nucleari innovativi, con particolare riguardo ai reattori nucleari di quarta generazione. Autore di oltre 20 articoli su rivista internazionale e di numerosi articoli a conferenze internazionali.

Daniele Martelli

Ha conseguito la laurea in Ingegneria Aerospaziale presso l'Università di Pisa nel 2009. A partire dallo stesso anno ha iniziato a collaborare, attraverso la società spin-off ACTA, con il DIMNP per analisi di fluidodinamica computazionale nell'ambito dell'ingegneria nucleare. Nel biennio 2010-2011 ha usufruito di una borsa di ricerca presso il DIMNP riguardante l'analisi del comportamento termoidraulico dei sistemi di refrigerazione dei reattori nucleari refrigerati a metallo liquido. Da gennaio 2012 è iscritto al corso di dottorato in "Ingegneria Nucleare e Sicurezza Industriale" in svolgimento presso il DIMNP dell'Università di Pisa. La sua attività di ricerca è principalmente incentrata sullo studio dei fenomeni di scambio termico in regime di convezione naturale e mista per reattori nucleari refrigerati a metallo liquido pesante.